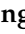



Article

Analysis of Energy Consumption and Economy of Regional Gas Tri-Supply Composite System

Mingyu Deng ¹, Yuxi Chen ², Jun Lu ¹ , Hao Shen ¹, Haibo Yang ^{3,*}  and Jie Yuan ³

¹ School of Civil Engineering, Chongqing University, Chongqing 400045, China; 202316021188t@stu.cqu.edu.cn (M.D.); lujun@cqu.edu.cn (J.L.)

² Department of Building Environment and Energy Engineering, The Hong Kong Polytechnic University, Kowloon, Hong Kong, China; cc_cc2002@icloud.com

³ Nuclear Industry Jingxiang Construction Group Co., Ltd., Huzhou 313000, China

* Correspondence: 13867282992@139.com (H.Y.); lishengyu.mr@gmail.com (S.L.)

Abstract: With the development of Chinese society, there is an increasing demand for emissions reduction and the stable operation of the power grid. Regional comprehensive energy supply systems have entered the public's view owing to their advantages of reducing capacity, unified dispatch, improving efficiency, and reducing energy consumption. This paper focuses on a system under construction in Chongqing, which adopts a combined gas tri-supply (combined cooling, heat, and power, CCHP) and dynamic ice storage cooling system as the research object. By establishing a mathematical model for the simulation research, this study examines the start–stop priority sequence of the gas tri-supply subsystem and the heat pump subsystem under the ice storage priority strategy in winter and summer and proposes corresponding optimization solutions. By comparing the annual operating energy consumption of the system, we conclude that the gas tri-supply composite system has good economic efficiency and peak-shaving capability, indicating that regional gas tri-supply composite systems have great application potential in the future. The proposed optimized operation strategy and simulated energy consumption calculation provide theoretical guidance for the construction and operation of both this project and similar projects.

Keywords: composite system; CCHP; ice storage and cold water storage; peak shaving; control strategy



Citation: Deng, M.; Chen, Y.; Lu, J.; Shen, H.; Yang, H.; Li, S.; Yuan, J. Analysis of Energy Consumption and Economy of Regional Gas Tri-Supply Composite System. *Buildings* **2024**, *14*, 1390. <https://doi.org/10.3390/buildings14051390>

Academic Editor: Charalampos Baniotopoulos

Received: 11 April 2024

Revised: 1 May 2024

Accepted: 9 May 2024

Published: 13 May 2024



Copyright: © 2024 by the authors. Licensee MDPI, Basel, Switzerland. This article is an open access article distributed under the terms and conditions of the Creative Commons Attribution (CC BY) license (<https://creativecommons.org/licenses/by/4.0/>).

1. Introduction

As a response to climate change, the reduction of emissions and the enhancement of energy efficiency are important strategies for countries around the world [1,2]. Integrated energy systems that can achieve the complementary utilization of multiple forms of energy and cascading utilization have become a research focus. Additionally, integrated energy systems that supply “cold, heat, electricity, and gas” can effectively address the issue of mismatch between power supply and demand in China, aiding in electricity peak shaving [3]. Under the strategic goal of comprehensive carbon reduction, natural gas, as a high-quality, efficient, and low-carbon clean energy source, demonstrates unparalleled advantages over other energy sources [4]. Moreover, with the completion of a large number of natural gas infrastructure projects in China, the reception and storage capacity of the country's natural gas has significantly improved. Therefore, the gas tri-supply subsystem and dynamic ice storage subsystem have tremendous development potential in China. Researching the energy consumption and economic performance of this composite system holds significant reference value for the operation and construction of practical projects.

1.1. Current State of Research on CCHP Systems

1.1.1. Current State of Research on CCHP System Performance

China has entered the phase of practical application and development implementation for CCHP technology. Many scholars have researched the development prospects of

employing CCHP systems in China and the operational status of existing projects. Xian Jingjiang et al. [5] summarized the development status of CCHP in Guangdong, finding that projects such as the Guangzhou University Town Distributed Energy Station and Guangzhou Supercomputer distributed energy demonstrate good economic benefits and energy-saving potential. Liu Qingrong et al. [6] investigated the development status of gas distributed energy in Shanghai, concluding that it holds promising development prospects in the city. Li Zishen et al. [7] analyzed two typical gas-fired distributed energy projects, one in Shanghai and the other in Tianjin, respectively, and concluded that both projects yielded favorable economic and social benefits. Zhang Liyuan [8] et al. investigated an integrated MG with CCHP systems, designed to efficiently supply energy demands while considering the environmental impacts of generation units associated with CO₂ emissions. In the system, the integrated CCHP-based MG incorporates a power-to-gas(P2G) technology, which enhances the system performance and reduces carbon emissions.

1.1.2. Current State of Research on the Operational Optimization of CCHP Systems

Focusing on the control challenges of large gas triple-supply systems, which exhibit complex coupling across various aspects, extensive research has been conducted in this domain. Ren et al. [9] developed a mixed-integer nonlinear programming model aimed at minimizing the annual cost, thereby determining the optimal configuration and operation strategy for the distributed energy system. Wu et al. [10] optimized the operation scheme of the combined cooling, heating, and power (CCHP) supply system to enhance energy-saving and cost-saving rates. Nong Jing et al. [11] proposed a hierarchical microgrid coordinated control strategy tailored to various time scales and implementation functions for CCHP systems, ensuring smooth control mode switching and output power transitions. Tu Qiang et al. [12] investigated multi-agent coordination issues in distributed energy systems and proposed a distributed coordination two-level optimization framework and strategy. This approach addressed optimal decision-making and energy scheduling challenges in distributed energy systems, effectively enhancing the economic performance of each agent utilizing the system. Chu Shangling [13] optimized a micro-gas turbine coupled with a combined LCPV/T and CCHP system by numerical simulation and proposed an optimal control strategy based on power load. The energy efficiency improvement of the system could be maintained above 25%.

1.2. Current State of Research on Ice Storage Systems

1.2.1. Current State of Research on the Performance of Ice Storage Technology

In the heating, ventilation, and air-conditioning (HVAC) field, energy storage systems are widely utilized to mitigate substantial peak–valley disparities in the electrical grid and efficiently absorb surplus electricity from renewable sources. An increasing number of large-scale energy facilities are adopting energy storage air-conditioning technology [14]. Among these, ice storage technology, which accumulates energy during off-peak hours when electricity prices are low and releases it during periods of peak demand in the daytime, has garnered considerable attention in the industry due to its substantial storage capacity and robust peak-shifting capabilities [15–17]. Research on this technology is becoming increasingly extensive both domestically and internationally. In current practical applications, a water thermal storage system (a shared tank for cooling and heating) is employed to align with the summer demand for the ice storage system and avoid its idleness during winter.

Chen Ruibin et al. [18] investigated the cold source system of an office building complex in Guangzhou and found that the ice storage system can decrease the unit configuration capacity while demonstrating effective peak-shifting and valley-filling performances and economic benefits. Xu Peng et al. [19] conducted research on the ice storage system of an office building in Beijing. Based on Beijing's peak and off-peak electricity pricing policy and the measured data from the ice storage system, they performed a comprehensive economic analysis and concluded that utilizing the ice storage system in Beijing yields significant eco-

conomic advantages. Fan Ying et al. [20] used a representative ice storage system in an office building in Zhejiang Province as a case study to determine the peak load reduction and valley-filling capacity of the system. They also calculated the coal consumption reduction resulting from the increased load rate of the power grid due to the system's peak load reduction and valley-filling performance, concluding that the ice storage system significantly contributes to emissions reduction in the power sector. Concerning water thermal storage systems, Hasnain S.M. et al. [21] selected a building in Saudi Arabia to investigate both water heat storage air-conditioning and phase change storage air-conditioning systems. The results demonstrated their substantial impact on grid balancing, with the ability to reduce peak cold load by approximately 35% and peak electricity consumption by about 15%. Hu Tao et al. [22] selected the water heat storage + ground source heat pump composite system as the subject of their experimentation. They derived optimization measures through actual measurements and data simulation analysis. Following implementation, the COP value of the heat pump rose from 3.0 to 4.5, resulting in substantial operational cost savings during peak shifting and valley filling, with a savings ratio of 21.8%. Dai Wei [23] et al. developed a combined cooling and power dispatch (CCPD) model, in which ice storage is used for energy storage. Through numerical simulation, it was concluded that the ice storage system can decouple the cooling capacity from the cold load and better utilize the wind power. At the same time, the ice storage system can convert wind energy into cold energy storage.

1.2.2. Research Status on the Operational Optimization of Ice Storage Cooling Systems

While ice storage cooling systems can effectively shift electrical load peaks and fill valleys, the effects of operational strategies, such as prioritization and allocation, during actual operation on the system's performance are crucial and cannot be overlooked. Consequently, the economic potential of ice storage cooling systems is significant, and there is considerable room for operational optimization. Scholars have undertaken research in this field.

Cao Jianwei et al. [24] utilized a significant number of ice storage air-conditioning clusters as the foundation to establish a framework for integrating ice storage air-conditioning clusters into micro-grid economic scheduling. They also introduced an optimal control strategy for the ice storage system. In comparison to conventional air conditioners and lithium batteries, utilizing an ice storage system for consuming renewable energy power at the user end is more economical. He Houyu et al. [25] enhanced the control strategy of the ice storage system aiming to optimize the economy on both the power source side and the load side. This proposed strategy significantly enhanced the performance of peak shifting and the capacity for absorbing renewable energy in the ice storage system. Wang Xiao et al. [26] developed a data-driven model for predicting building cooling loads and subsequently optimized the control model of the ice storage system based on the predicted cooling load. This approach facilitates dynamic control of the ice storage system and consequently effectively reduces the energy costs associated with the system. Wu Lei et al. [27] formulated a mathematical model for ice storage and release within the ice storage system. They examined the potential of the ice storage system to respond to power grid regulation under four typical load rates and optimized the system with the objective of maximizing demand for power grid regulation. Implementing this control strategy can significantly enhance the demand response potential of the ice storage system, mitigate peak loads, fill valleys within the power grid, and yield greater economic benefits for end users.

1.3. Research Status on Composite Systems

Composite energy supply systems are frequently encountered in district energy station projects. These district-level systems necessitate substantial investment due to their large installed capacities and the involvement of numerous complex pipelines and equipment. As such, it is crucial to calculate operational energy consumption and develop optimization strategies for district energy systems. Doing so is essential for maximizing their advantages

and achieving greater overall benefits. In recent years, there has been a growing body of research in this area undertaken by scholars.

Shi Qian [28] proposed a system structure that can comprehensively utilize multiple green energy sources and realize flexible power consumption through energy storage. The article optimized the control strategy of this system structure by establishing a mathematical model, and the optimized control strategy can improve the utilization rate of green energy and the stability of system operation. Professor Lu Jun's team [29,30] at Chongqing University analyzed and optimized various composite energy supply systems, including CCHP systems, and composite systems integrating river source heat pumps. Their research encompassed various optimization analysis aspects, including operational strategies, modes of operation, inlet and outlet water temperatures, temperature differences between supply and return water, and grid connection methods. Additionally, they conducted comparisons between strategies for ice storage cooling and water source heat pump composite systems, as well as between different thermal storage modifications. Wang Jun et al. [31] systematically reviewed and investigated the coupled energy storage technology of distributed energy systems. They concluded that the integration of ice and cold water storage technology with traditional distributed energy systems has reached the stage of commercial application, demonstrating favorable operational effects and economic benefits. Qin Yuan et al. [32] investigated a building-type distributed energy station in central China, comparing two schemes utilizing traditional air-conditioning systems and ice storage systems within the station. They concluded that due to significant fluctuations in the load of the building distributed energy station throughout seasons and day–night cycles, an energy storage system is necessary. When the peak-to-valley electricity price ratio reaches 3:1, the ice storage air-conditioning system exhibits superior economic benefits. Wang Xueqin et al. [33] focused on the cooling mode of a building-type distributed energy station in Shanghai, establishing and comparing two configuration schemes: ice storage and water storage. They conducted a comprehensive analysis of the operation mode and economy of each scheme and concluded that the water storage system of the distributed energy station offered better overall benefits. Wang Hui et al. [34] analyzed mathematical models for the CCHP system, energy storage system, and heat pump system of a distributed energy station. Considering policy incentives and energy costs, they proposed an optimal control strategy aimed at maximizing energy cost savings. The implementation of this strategy resulted in superior economic benefits for the distributed composite system. Yu Chunyao et al. [35], using actual measured data from established district energy systems in Shanghai, analyzed various subsystems and optimized their operating modes. They found that the system's comprehensive energy utilization rate could exceed 80% under both cooling and heating conditions, with relatively low average energy costs, leading to significant economic benefits. Jia Jiandong et al. [36] developed regional integrated energy systems coupled with renewable energy, energy storage, and inter-station energy sharing. Through numerical simulation, different operation strategies are compared, and finally an optimization strategy is proposed. Compared with other regional energy systems, the energy system developed in this study has a better energy-saving effect under the optimization strategy.

1.4. Issues and Practical Significance

Currently, there is abundant research on the analysis of energy consumption and control strategies for both CCHP systems and ice storage cooling systems. However, research on composite district energy systems remains scarce. Many large-scale systems currently face challenges such as high energy consumption, inadequate energy storage, and poor economic performance due to the lack of scientific operating strategies. Therefore, it is crucial to establish the best operational strategies and control systems, while also determining the priorities for the operation of each subsystem. Additionally, it is worthwhile to pay attention to the energy consumption and economic performance of composite systems when employing the optimized operational strategies.

Therefore, this paper aims at optimizing the control strategies of the regional gas tri-supply composite system with an emphasis on analyzing economic and energy consumption performance. The research on optimizing the operational strategies of this system can effectively reduce the investment in electric power construction and enhance the economic performance of composite systems. This study is of theoretical significance in providing guidance for similar systems. Compared to previous studies, this paper focuses on the regional gas tri-supply composite system. With the aim of economic optimization, strategies are optimized, and the economic superiority of the optimized strategies is demonstrated through numerical simulations.

Section 2 of this paper presents the load results calculated by DEST and shows the system equipment configuration of the project based on the load results. Section 3 establishes the mathematical modeling of the subsystems of the triplex composite system. Section 4 analyzes the control strategy, simulates the system's energy efficiency throughout the year under the optimized control strategy, and analyzes the results in terms of economy, peak-shifting and valley-filling capacity, and power production capacity. Section 5 presents the conclusions obtained through this study.

2. Project Overview and Load Analysis

2.1. Project Overview

This project entails the development of a city area within Chongqing, situated in the western region adjacent to the Jialing River. The total construction area covers approximately 13,857.00 million m^2 , including a commercial building area of about 995,900.00 m^2 and a residential construction land area of about 389,800.00 m^2 . Through the regional energy station, the buildings in this project undergo cooling and heating. The land area of the energy station encompasses 2000.00 m^2 , with a total building area of 8027.76 m^2 . The geographical location of the energy station is depicted in Figure 1.

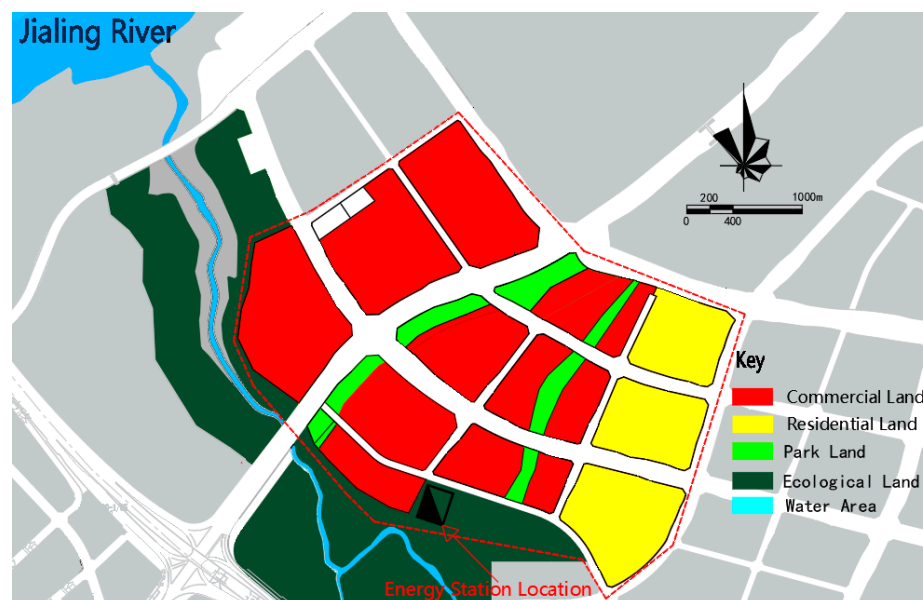


Figure 1. Energy station planning diagram.

2.2. Project Load Analysis

Utilizing DeST-C software, the annual cold and heat loads for both the commercial and residential buildings within the project are simulated, with unified cooling and heating provided by the energy station.

2.2.1. Analysis of Summer Cooling Load

According to the simulation, the hourly cooling load distributions for both commercial and residential buildings are depicted in Figures 2 and 3. The cooling period spans from 1 June to 1 October each year, totaling 122 days. The maximum cooling load for commercial buildings is 139.4 MW, and for residential buildings, it is 24.5 MW.

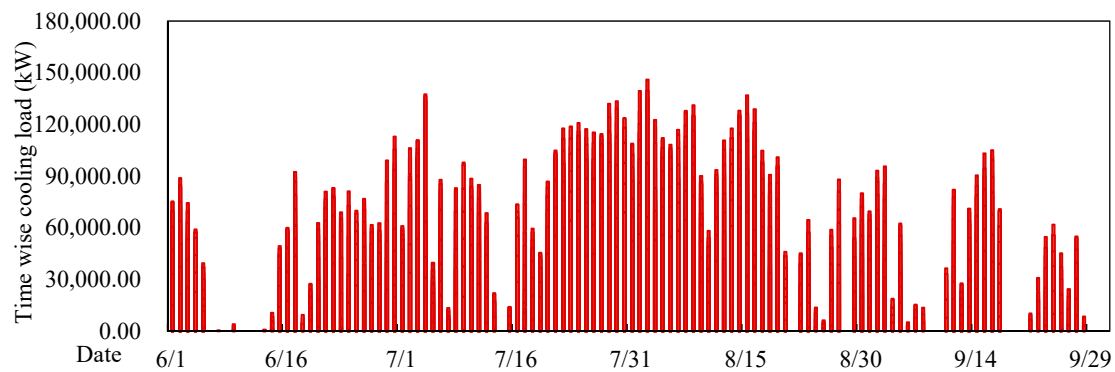


Figure 2. Annual daily cooling load of commercial buildings in the power supply area.

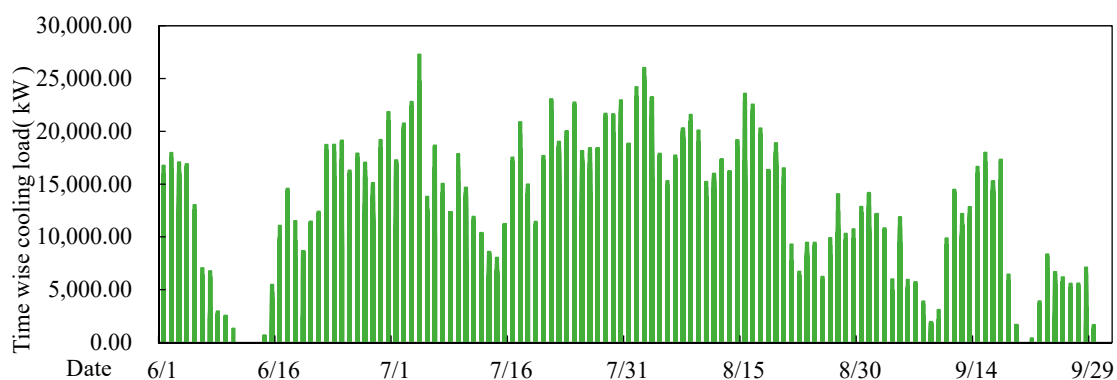


Figure 3. Annual daily cooling load of residential buildings in the power supply area.

According to relevant engineering experience, the simultaneous use coefficient in summer is 0.65, resulting in a cooling load of 106.59 MW for the energy supply area. Additionally, the cooling load per unit area of the building is determined to be 76.92 W/m²; refer to Table 1.

Table 1. Cooling load calculation table of energy supply area.

Building Type	Area (Ten Thousand m ²)	Indicator of Cold Load per Unit Building Area (W/m ²)	Building Cooling Load (kW)	Coefficient of Simultaneous Use	Area Cooling Load (kW)	Area Cooling Load Index (W/m ²)	Percentage (%)
Commercial buildings	99.59	140.01	139,435.96	0.65	106,593	76.92	85.02
Residential buildings	38.98	62.99	24,553.50				14.98

Based on the load simulation results, typical daily cooling load values are obtained. Due to the significant disparity between commercial and residential loads, the hourly cooling load on 4 July (the time of maximum cooling load occurrence for commercial buildings) is selected for further investigation; refer to Figure 4.

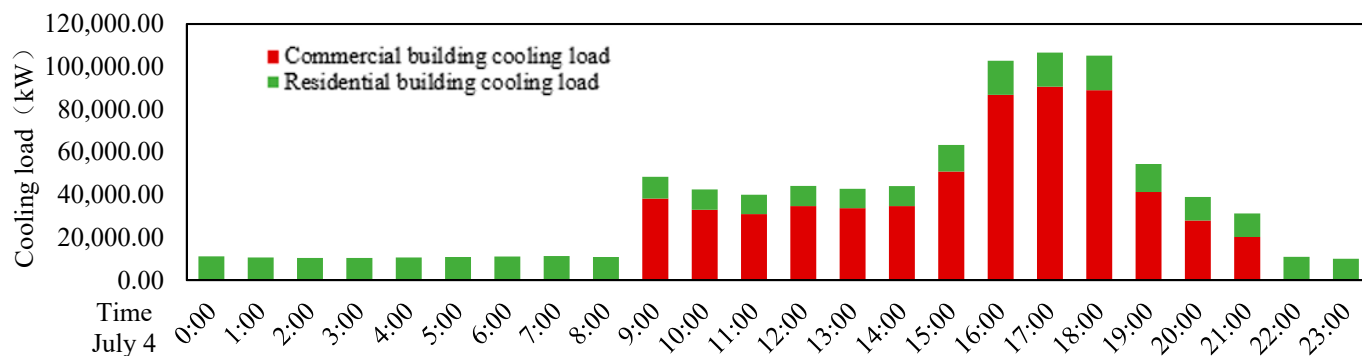


Figure 4. Hourly cooling load of one day in the energy supply area.

To simulate energy consumption effectively, we calculate the annual occurrence frequency of the load rate, as illustrated in Table 2. The cold load rate predominantly falls between 25% and 50%, constituting 52 days within the cooling season, which accounts for 42.62% of its duration. The operational time at 75% to 100% load is relatively low, totaling only 8 days per year.

Table 2. Statistical table of the annual cooling load rate.

Load Factor	June	July	August	September	Total	Proportion of Each Load Rate
%	days	days	days	days	days	%
75~100%	0	4	3	1	8	6.56%
50~75%	3	13	9	2	27	22.13%
25~50%	15	12	15	10	52	42.62%
0~25%	12	2	4	17	35	28.69%

2.2.2. Heat Load Analysis in Winter

Separate thermal load simulations are conducted for commercial and residential buildings within the power supply area. The outcomes of these simulations are depicted in Figures 5 and 6. Central heating is operational from 1 December to 28 February, spanning 89 days. For commercial buildings, the maximum heat load reaches 57.3 MW, whereas for residential buildings, it is 14.3 MW.

According to relevant engineering experience, the simultaneous use coefficient in winter is determined to be 0.65, resulting in a calculated heat load of 46.61 MW for the energy supply area. Additionally, the cooling load per unit area of the building is measured at 33.63 W/m²; refer to Table 3.

Table 3. Heating load calculation table of energy supply area.

Building Type	Area (Ten Thousand m ²)	Indicator of Heat Load per Unit Building Area (W/m ²)	Building Heating Load (kW)	Coefficient of Simultaneous Use	Area Heating Load (kW)	Area Heating Load Index (W/m ²)	Percentage (%)
Commercial buildings	99.59	57.58	57,343.92	0.65	46,613	33.63	79.96
Residential buildings	38.98	36.86	14,368.03				20.04

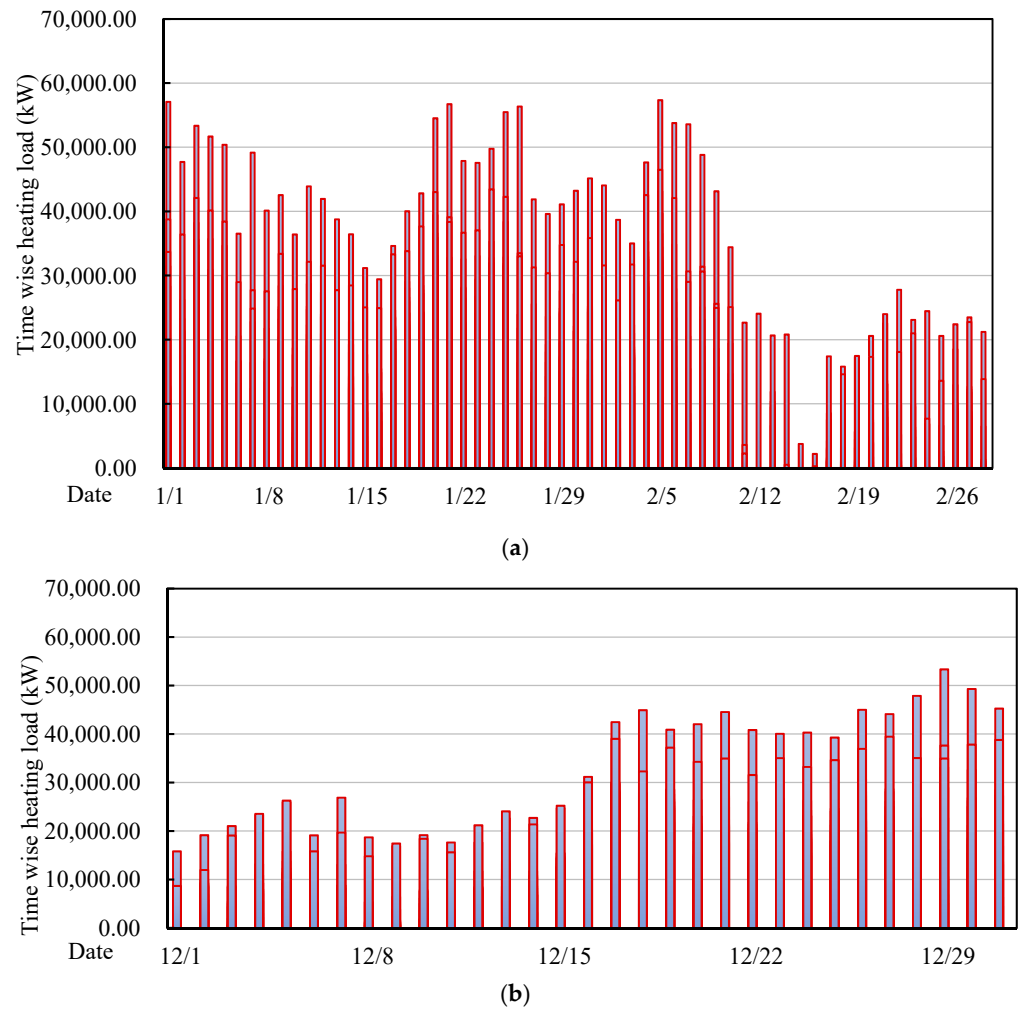


Figure 5. Annual daily heat load of commercial buildings in the power supply area of (a) 1 January through 28 February and (b) 1 December through 31 December.

Subsequently, the load simulation results yield the typical time-down heat load value. Given the substantial difference in load between commercial and residential buildings, the time-down heat load is analyzed on February 5th, which coincides with the peak heat load occurrence for commercial buildings (see Figure 7 for further investigation).

Simulation statistics of the building heat load rate in the energy supply area and the statistical results are shown in Table 4. Due to the continuity of heating, the heat load rate is mainly concentrated between 25% and 75%.

Table 4. Statistical table of the annual heat load rate.

Load Factor	December	January	February	Total	Proportion of Each Load Rate
%	days	days	days	days	%
75~100%	3	6	3	12	13.33%
50~75%	10	18	7	35	38.89%
25~50%	15	5	16	36	40.00%
0~25%	3	2	2	7	7.78%

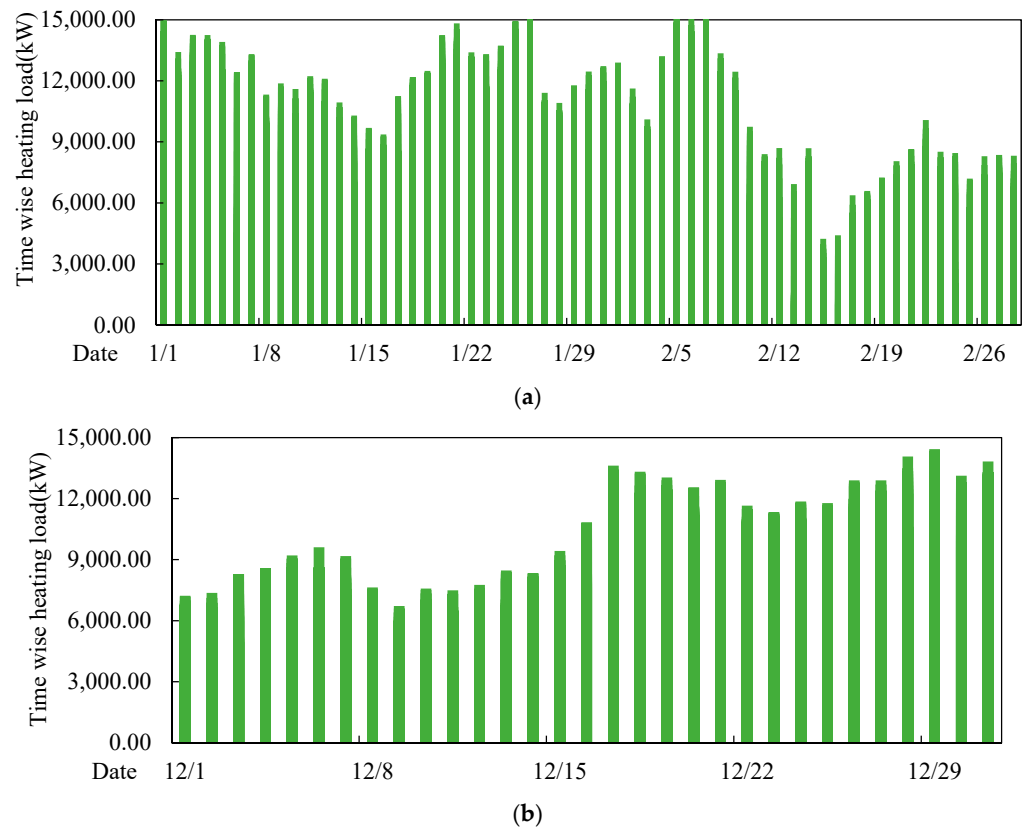


Figure 6. Annual daily heat load of residential buildings in the power supply area of (a) 1 January through 28 February and (b) 1 December through 31 December.

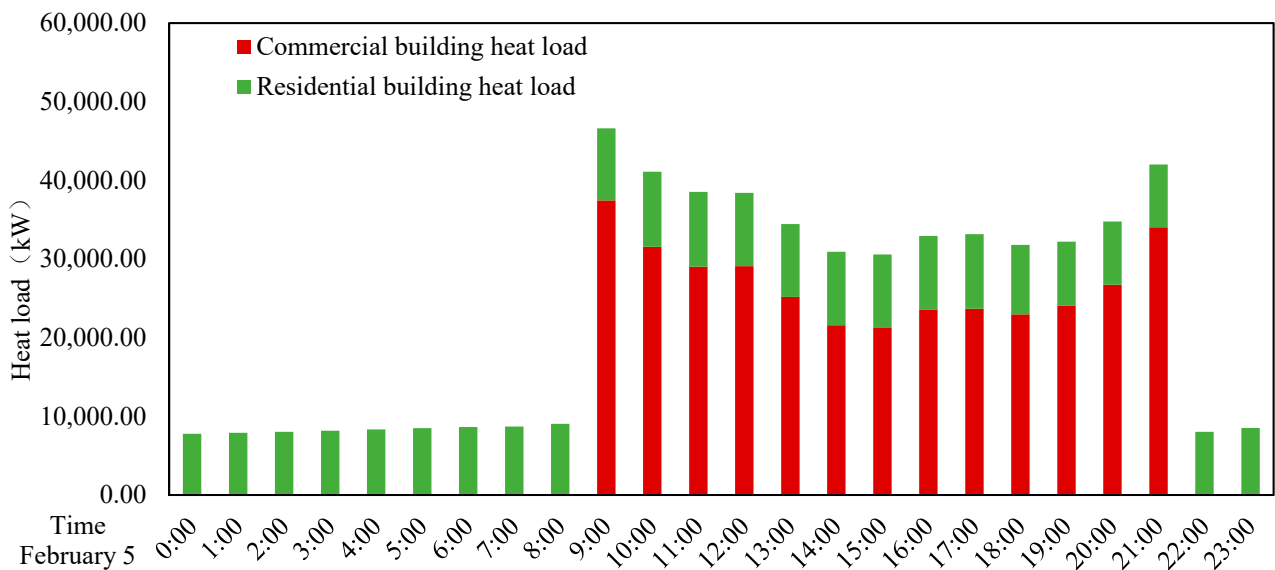


Figure 7. Hourly heating load of one day in the energy supply area.

2.3. Device Configuration of the Gas Tri-Supply Composite Source System

In this project’s summer operations, a combination of a variable frequency conversion centrifugal chiller, gas triple-water-supply system, water source heat pump, and dynamic ice storage system is employed for cooling. During winter, the heating system utilizes the gas triple-supply system, water source heat pump system, and water heat storage system in combination.

The energy station is equipped with two gas-fired boilers, each with a heat production capacity of 12.6 MW; five frequency conversion centrifugal double-duty units, providing a single refrigeration capacity of 8438 kW and an ice production capacity of 6680 kW; one frequency conversion centrifugal refrigeration unit, delivering a single refrigeration capacity of 8438 kW; five water source heat pump units, offering a single refrigeration capacity of 4280 kW and a single heat production capacity of 3520 kW; two gas-fired internal combustion engines, each with a power generation capacity of 2000 kW; paired absorption units, providing a single refrigeration capacity and heat production capacity of 1745 kW and 1883 kW, respectively; the ice storage device has a maximum cold storage capacity of 213,200 kWh and a maximum heat storage capacity of 78,000 kWh during winter. The total length of the energy station's energy supply pipeline to the energy supply area is approximately 10,037 m. Table 5 details the configuration of the energy station units.

Table 5. Equipment capacity configuration table of the gas tri-supply composite system.

Equipment	Host Specifications			Set Number
Double-condition unit	Refrigeration condition	Refrigeration capacity (kW/unit)	8438	5
		Power consumption (kW/unit)	1337	
		COP	6.31	
	Ice-working condition	Ice volume (kW/set)	6680	
		Power consumption (kW/unit)	1542	
		COP	4.33	
Centrifugal unit	Refrigeration condition	Refrigeration capacity (kW/unit)	8438	1
		Power consumption (kW/unit)	1337	
		COP	6.31	
Gas fired boiler	Heating condition	Heat (kW/set)	12,600	2
		Power consumption (kW/unit)	46	
		Gas consumption/(Nm ³ /h/set)	1186	
Water source heat pump	Refrigeration condition	Refrigeration capacity (kW/unit)	4280	5
		Power consumption (kW/unit)	826	
		COP	5.18	
	Heating condition	Heat (kW/set)	3520	
		Power consumption (kW/unit)	920	
		COP	3.83	
Gas internal combustion engine		Power generation (kW/unit)	2000	2
		Generating efficiency (%)	43.7	
		Utilization used heat (kW/set)	2000	
		Heat efficiency (%)	43.7	
		Gas consumption (Nm ³ /h/set)	482	
Absorption unit		Refrigeration capacity (kW/unit)	1745	2
		Heat (kW/set)	1883	
		Power consumption (kW/unit)	9.9	

Allocation Analysis of Gas Tri-Supply Composite System

During the summer cooling period, each system's total cooling capacity at full load is 106.59 MW, aligning with the cooling load. Dual-operating-condition units and centrifugal units have a high cooling COP in summer and account for approximately 47% of the cooling load. The ice storage system provides a maximum cooling capacity of 30,460 kW per hour and a peak-shifting capacity of 213,200 kWh. The cooling stage of ice storage, which can handle 28.74% of the cooling load, releases cooling during peak load periods of the day, thereby achieving a peak-shifting effect and yielding substantial economic benefits. The water source heat pump unit utilizes renewable energy for both summer cooling and winter heating, with a high COP. The absorption unit accounts for 3.29% of the cooling load while

also generating electricity. Meanwhile, Table 6 illustrates the detailed breakdown of each unit's cooling capacity.

Table 6. Proportion of equipment for composite cold and heat source system.

Equipment	Single Cooling Capacity (kW)	Total Cooling Capacity (kW)	The Portion of Single Cooling Capacity	Total Refrigeration Ratio
Double-working-condition unit	8438	42,190	7.96%	39.81%
Centrifugal unit	8438	8438	7.96%	7.96%
Heat pump unit	4280	21,400	4.04%	20.19%
Absorption unit	1745	3490	1.65%	3.29%
Ice storage system		30,460		28.74%

During the winter heating period, the heat pump unit is designed based on the summer cooling load. Each system produces a total heat output of 63.5 MW when operating at full capacity during winter, with a heat load of 46.61 MW. During winter, the cold storage tank of the summer dynamic ice storage system is utilized for heat storage, capable of handling 36.47% of the heat load, thereby facilitating peak shifting and yielding economic benefits. The gas-fired boiler configuration, which accounts for 54.07% of the heat load, bears the majority of the heat load throughout the day. The river water source heat pump handles 37.76% of the heat load during winter, with the unit exhibiting high heating efficiency. The absorption unit handles 8.08% of the heat load while also generating electricity. The detailed breakdown of heat production for each equipment is presented in Table 7.

Table 7. Proportion of equipment in composite cold and heat source system.

Equipment	Single Heat (kW)	Total Heat Production Rate (kW)	Single Unit Heat Production to Heat Load Ratio	Total Heat Production to Heat Load Ratio
Gas fired boiler	12,600	25,200	27.03%	54.07%
Heat pump unit	3520	17,600	7.55%	37.76%
Absorption unit	1883	3766	4.04%	8.08%
Water storage system		17,000		36.47%

2.4. Traditional Cold and Heat Source Configuration of Energy Station

The conventional cold and heat sources are configured using chillers and boilers. The cold load in summer is 106.59 MW, and the heat load in winter is 46.61 MW, with the system configured accordingly. Table 8 presents the detailed parameters of the equipment.

Table 8. Capacity configuration table of traditional cold and heat source system equipment.

Equipment	Host Specifications		Set Number
Centrifugal unit 1	Refrigeration condition	Refrigeration capacity (kW/unit)	8438
		Power consumption (kW/unit)	1337
		COP	6.31
Centrifugal unit 2	Refrigeration condition	Refrigeration capacity (kW/unit)	5626
		Power consumption (kW/unit)	897
		COP	6.27
Gas boiler 1	Heating condition	Heat (kW/set)	12,600
		Power consumption (kW/unit)	46
		Gas consumption (Nm ³ /h/unit)	1186
Gas boiler 2	Heating condition	Heat (kW/set)	10,500
		Power consumption (kW/unit)	37
		Gas consumption (Nm ³ /h/unit)	1016

3. Energy Consumption Model of the Composite Energy System

This project adopts a composite energy system, which can be divided into four subsystems: a triple-supply subsystem consisting of a gas internal combustion engine + lithium bromide absorption unit, an ice storage subsystem composed of a frequency conversion centrifugal double unit + dynamic ice storage, a heat pump subsystem consisting of a water source heat pump unit, and a boiler subsystem composed of a gas boiler.

3.1. Mathematical Model of Gas Tri-Supply Subsystem

The gas tri-supply subsystem operates by consuming gas to generate electricity efficiently. The absorption unit utilizes waste heat from internal combustion engine flue gas and high-temperature cylinder liner water to provide refrigeration. Therefore, establishing a model to assess the cooling capacity, heat production, power generation, and gas consumption of the triple-supply subsystem is imperative.

1. Mathematical model of the gas internal combustion engine

Referring to the relevant literature [29], the main performance indicators involved in the dynamic model of the internal combustion engine include generation power (P_e), generation efficiency (η_e), available surplus heat (P_h), thermal efficiency (η_h), air consumption (G_N), load ratio (N), etc. The two “MWM” gas internal combustion engines selected for this project are analyzed, whose models are MWM 2000, and their related performance parameters are shown in Table 9.

Table 9. Gas internal combustion engine performance parameters table.

Equipment	Power Generation kW	Generating Efficiency %	Utilizable Waste Heat kW	Heat Efficiency %	Unit Efficiency %	Gas Consumption Nm ³ /h	Exhaust Smoke Level kg/h	Exhaust Smoke Temperature °C	Cylinder Water Heat kW
MWM 2000	2000	43.7	1978	43.2	86.9	482	10,842	414	1005

(1) Gas consumption of gas internal combustion engine

Under different load conditions, the gas consumption of the gas internal combustion engine is different. Combined with the relevant literature [37], it can be seen that the gas consumption of the gas internal combustion engine and the unit load exhibit a basically linear relationship. According to the relevant parameters provided by the unit manufacturer, when the load rate of the unit is 100%, 75%, and 50%, the gas consumption of the unit MWM 2000 is 482, 372 and 261 Nm³/h. By fitting the data with software, Equations (1) and (2) show the relationship of gas consumption (G_N) and load rate (N). The relationship curve between the unit gas consumption and load rate is shown in Figure 8.

$$G_{N1} = G_{N2} = 440\overline{N}_1 + 42 \quad (1)$$

$$G_N = G_{N1} + G_{N2} = 440\overline{N}_1 + 440\overline{N}_2 + 84 \quad (2)$$

(2) Power generation of gas internal combustion engine

According to the sample parameters and the literature [29], when the load rate of the gas-generating unit is less than 50%, the power generation efficiency of the generator set is stable, and when the load rate is higher than 50%, the power generation efficiency fluctuates significantly. Therefore, the load rate of the gas unit should be kept higher than 50% in the operation stage. When the load rate is greater than 50%, a quadratic function is fitted to the power generation efficiency (η_e) and the load rate (N), and the fitting formula is given in Equation (3). The relationship curve between the power generation efficiency and the load rate of the unit is shown in Figure 9.

$$\eta_{e1} = \eta_{e2} = -0.072\overline{N}_1^2 + 0.178\overline{N}_1 + 0.331 \quad (3)$$

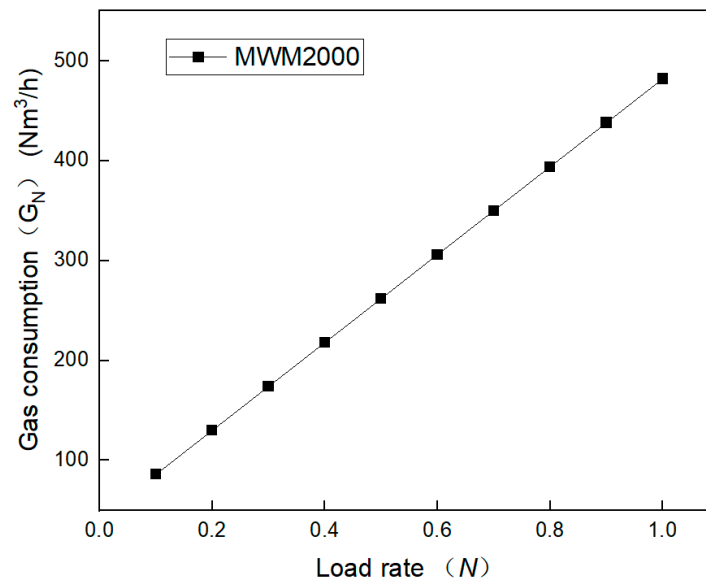


Figure 8. Relationship between gas consumption and unit load rate.

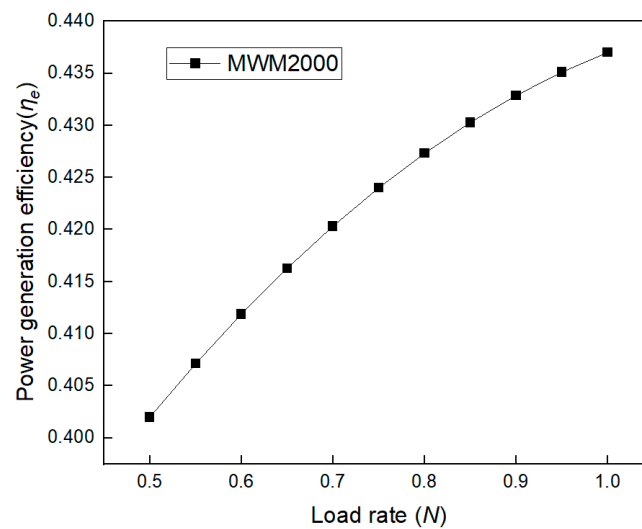


Figure 9. Relationship between power generation efficiency and load rate of the unit.

The calorific value of the gas (q_g) is 9 kWh/Nm³. Combined with the gas consumption from Equation (1), Equation (4) shows the rule of generating capacity varying with load rate.

$$P_{e1} = P_{e2} = -300.96\bar{N}_1^3 + 715.312\bar{N}_1^2 + 1454.602\bar{N}_1 + 132.069 \quad (4)$$

(3) Thermal efficiency of the gas internal combustion engine

Due to the low load rate of the unit, the power generation efficiency of the unit will be reduced. In order to simplify the model, only the load rate of more than 50% is analyzed. The change in thermal efficiency (η_h) of unit MWM 2000 with the load rate change (N) is shown in Figure 10. It can be seen that the thermal efficiency of the gas internal combustion engine decreases with the increase in the load rate of the unit. A quadratic function is fitted to the data change in the thermal efficiency (η_h) and load rate (N) of the unit when the load rate is greater than 50% to obtain Equation (5).

$$\eta_{h1} = \eta_{h2} = -0.016\bar{N}_1^2 + 0.056\bar{N}_1 + 0.392 \quad (5)$$

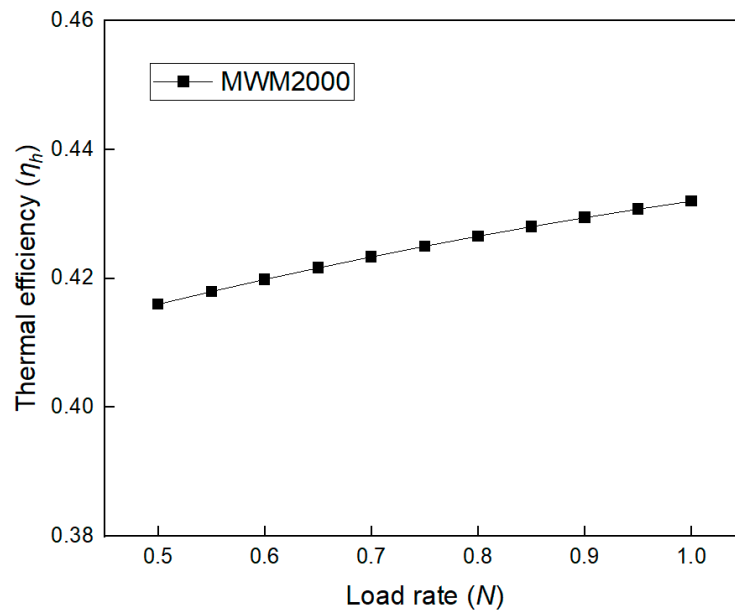


Figure 10. Relationship between thermal efficiency and load rate of the unit.

Similarly, the calorific value of gas (q_g) is 9.5 kWh/Nm^3 . Combined with the unit gas consumption from Equation (1), the available residual heat (Equation (6)) of the two units is obtained.

$$P_{h1} = P_{h2} = -66.88\bar{N}_1^3 + 227.696\bar{N}_1^2 + 1660.904\bar{N}_1 + 156.408 \quad (6)$$

(4) The flue gas temperature of the gas internal combustion engine

The thermal coefficient of the absorption unit is influenced by the temperature of the flue gas; therefore, a flue gas temperature model is established in this study. The exhaust temperature of unit MWM 2000 varies with the load, as illustrated in Figure 11, demonstrating a decrease as the load increases. Based on the manufacturer's data on flue gas temperature under different loads, Equation (7) is derived.

$$T_{Y1} = T_{Y2} = 32\bar{N}_1^2 - 168\bar{N}_1 + 550 \quad (7)$$

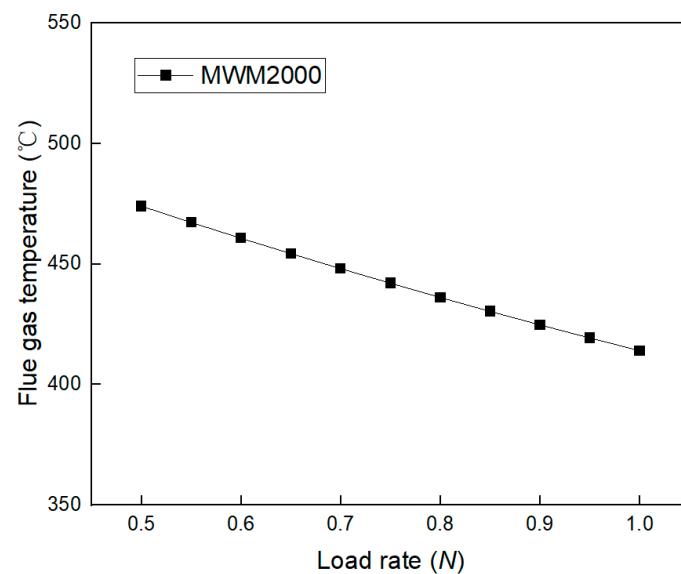


Figure 11. Relationship between smoke exhaust temperature and load rate.

2. Mathematical model of lithium bromide absorption unit

The lithium bromide absorption unit generator uses the waste heat of gas internal combustion engine flue gas and the waste heat of casing cylinder water to drive the lithium bromide absorption unit to supply cold and hot water to the air conditioning. Therefore, the refrigeration heat production of the lithium bromide absorption unit is related to the load rate of the internal combustion engine.

The units selected for this project are two BZHE150 Yuanda XII flue gas hot water lithium bromide absorption units. The detailed design performance parameters of the units are shown in Table 10. According to the selection manual and the data provided by the merchant, the dynamic mathematical modeling of the two units is conducted.

Table 10. Performance parameters table of lithium bromide absorption unit.

Equipment	Refrigerating Capacity	Heating Capacity	Cold Water Flow	Cold Water Temperature	Warm Water Flow	Warm Water Temperature	Cooling Water Flow	Cooling Water Temperature	Distribution Volume	Rated COP for Refrigeration	Rated COP for Heating
	kW	kW	m ³ /h	°C	m ³ /h	°C	m ³ /h	°C	kW		
BZHE 150	1745	1883	214	7/14	116	65/55	393	37/30	9.9	1.50	0.93

(1) Using waste heat for refrigeration

This study references the relevant literature [29] to establish the relationship between the thermal coefficient of the absorption unit, smoke exhaust temperature, and the inlet temperature of the cooling water for units of the same brand.

$$\zeta_C = 0.0009107T_Y - 0.01789T_{LQ} + 1.0796 \quad (8)$$

a. When the waste heat of the internal combustion engine is greater than the heat required for the full load refrigeration operation, the critical point is analyzed.

$$P_h \cdot \zeta_C = Q_{Br.L.r} \quad (9)$$

According to Equations (6)–(9), the change relationship of the cooling water temperature and the load rate of the internal combustion engine is obtained:

$$Q_{Br.L.r} = -1.949\bar{N}^5 + 16.868\bar{N}^4 + (1.1965T_{LQ} - 92.137)\bar{N}^3 + (110.31 - 4.0735T_{LQ})\bar{N}^2 + (2601.1 - 29.714T_{LQ})\bar{N} - 2.7981T_{LQ} + 247.2 \quad (10)$$

According to Equation (10), the inlet temperature of the cooling water is assigned to calculate the load rate of the gas internal combustion engine at the corresponding temperature. The calculation results are shown in Table 11.

Table 11. Load of internal combustion engine when the absorbing unit is fully loaded at different cooling water temperatures.

T _{LQ} (°C)	25	26	27	28	29	30	31	32	33	34
MWM 2000	0.85	0.86	0.88	0.90	0.93	0.94	0.97	0.99	1.0	1.0
BZHE 150	1.0	1.0	1.0	1.0	1.0	1.0	1.0	1.0	0.98	0.95

According to the above table, when the cooling water temperature is lower than 32 °C, the absorption unit can operate at full load. Under the standard working condition, the cooling water temperature of the absorption refrigeration unit is 30 °C, and when the load rate of the internal combustion engine is 94%, the absorption unit operates at full load. The project can consider the introduction of river water as cooling water. The low-temperature

cooling water can ensure that the load rate of the internal combustion engine is low and that the absorption unit operates at full load.

b. When the waste heat of the internal combustion engine is lower than the heat required for the full load operation of the absorption unit, the absorption unit is not replenished. A rated cooling water temperature of 30 °C is used for analysis and calculation:

$$\varepsilon_C = \frac{P_h \cdot \zeta_C}{Q_{Br.L.r}} \quad (11)$$

According to Equations (6)–(8) and Equation (11), the relationship between the load rate of the absorption unit and the load rate of the gas unit is:

$$\varepsilon_C = -0.00112\bar{N}^5 + 0.00967\bar{N}^4 - 0.0322\bar{N}^3 - 0.00681\bar{N}^2 + 0.980\bar{N} + 0.0936 \quad (12)$$

Therefore, the relationship between the cooling capacity of the absorption unit and the load rate of the internal combustion engine is:

$$Q_{Br.L} = -1.949\bar{N}^5 + 16.868\bar{N}^4 - 56.243\bar{N}^3 - 11.891\bar{N}^2 + 1709.7\bar{N} + 163.26 \quad (13)$$

(2) Using waste heat

Under heating conditions, the thermal system value is only related to the internal combustion engine flue gas temperature, as follows:

$$\zeta_H = 0.0005T_Y + 0.7074 \quad (14)$$

When the waste heat generated by the internal combustion engine is greater than the heat required by the full load heating operation of the absorption unit, the absorption unit operates at full load. The critical point:

$$P_h \cdot \zeta_H = Q_{Br.R.r} \quad (15)$$

By combining Equations (6) and (14), it can be calculated that the load rate of the gas internal combustion engine is close to 100%. The relationship between the heat load rate and the internal combustion engine is analyzed further:

$$\varepsilon_H = -0.000568\bar{N}^5 + 0.00492\bar{N}^4 - 0.0309\bar{N}^3 + 0.0460\bar{N}^2 + 0.860\bar{N} + 0.1192 \quad (16)$$

$$Q_{Br.R.r} = -1.0701\bar{N}^5 + 9.2611\bar{N}^4 - 58.255\bar{N}^3 + 56.675\bar{N}^2 + 1618.5\bar{N} + 153.66 \quad (17)$$

3.2. Mathematical Model of Dynamic Ice Storage Cooling System

This project employs a dynamic ice storage system to achieve a reduction in installed capacity and peak shifting. The subsystem utilizes an upstream series ice slurry cold storage configuration, consisting of 5 Midea CCWE 2400HVI10 units with a rated cooling capacity of 8438 kW and an ice storage capacity of 6680 kW. The cold storage capacity of the dynamic ice storage tank is 213,180 kWh. See Table 12 for the specific model of the unit.

Table 12. Parameters of the refrigeration unit under dual working conditions.

Equipment	Refrigerating Capacity kW	Ice Storage Capacity kW	Refrigeration Power kW	Ice Production Power kW	Refrigeration COP	Ice-Making COP
CCWE 2400HVI10	8438	6680	1337	1542.8	6.30	4.33

1. Dual-working-condition unit cold storage mode

According to the relevant parameters of the unit provided by the manufacturer and combined with the known engineering case experience [38], the system's $COP_{S,I}$ during the ice-making process of the dynamic ice storage system of the project is modeled. Due to the difference in the installed capacity of the unit, Equation (18) is obtained after the coefficient is corrected:

$$COP_{S,I} = -1.7610N_{S,I}^2 + 3.6111N_{S,I} + 1.8671 \quad (18)$$

Combined with the rated cooling capacity of the unit, the variation in the subsystem power consumption ($P_{S,I}$) with the load rate ($N_{S,I}$) under dynamic ice storage and ice-making conditions is analyzed and calculated, as shown in Equation (19):

$$P_{S,I} = (-0.00026N_{S,I} + 0.00028N_{S,I}^{-1} + 0.00054)^{-1} \quad (19)$$

2. Dual-operating-condition unit refrigeration mode

According to the parameters under refrigeration mode of the unit, the mathematical simulation modeling is carried out based on the change in $COP_{S,L}$ of the unit under refrigeration mode with the load ratio ($N_{S,L}$) of the dual-operation unit, and the relation Equation (20) is obtained:

$$COP_{S,L} = -4.8572N_{S,L}^2 + 8.723N_{S,L} + 2.3523 \quad (20)$$

Combined with the rated cooling capacity of the unit, the power consumption ($P_{S,L}$) under dynamic ice storage refrigeration conditions changes with the load rate ($N_{S,L}$), which is analyzed and calculated, as shown in Equation (21):

$$P_{S,L} = (-0.00058N_{S,L} + 0.00028N_{S,L}^{-1} + 0.00103)^{-1} \quad (21)$$

3. Ice storage pool melting ice

The peak regulation of the ice storage tank is set at 70% of the peak load. The maximum cooling capacity is 213,180 kWh and according to the empirical formula [39], the melting rate is fitted to obtain the melting rate formula of the ice storage tank:

$$Q_{I,t} = 94651 \times \left(1 - \frac{Q_{I,t,s}}{213180}\right) \quad (22)$$

$Q_{I,t}$ represents the maximum ice melting rate at time t; $Q_{I,t,s}$ represents the cooling capacity of melted ice at time t.

3.3. Mathematical Model of the Heat Pump Subsystem

This project employs river water source heat pumps and selects 5 Simpson SDR-46500S/LR4 units with a rated cooling capacity of 4280 kW and a heating capacity of 3520 kW. Refer to Table 13 for detailed design performance parameters. The operating conditions of the two units are mathematically modeled based on the selection manual and data provided by the manufacturer.

Table 13. Performance parameter table of the heat pump unit.

Equipment	Operating Mode	Rated Capacity kW	Rated Input Power kW	Cold/Hot Water Flow Rate m ³ /h	Cold/hot Water Inlet Temperature °C	Source Water Rate of Flow m ³ /h	Source Water Temperature °C	COP
SDR-46500S/LR4	refrigeration	4280	826	736	12/7	878	30/35	5.18
	heating	3520	920	736	40/--	878	0/-3	3.83

1. Heat pump unit refrigeration

According to the measured data of the engineering cases [30], in order to keep the heat pump unit operating more efficiently, the load rate should be kept between 50% and 100%. By fitting and modifying the performance parameters of the unit, the relationship between $COP_{H,L}$ and the load ratio ($N_{H,L}$) of the heat pump system is obtained as follows:

$$COP_{H,L} = -15.6394N_{H,L}^2 + 25.7264N_{H,L} - 5.2979 \quad (23)$$

Based on the rated cooling capacity of the unit, the power consumption ($P_{H,L}$) change with the load rate ($N_{H,L}$) of the heat pump unit is analyzed and calculated:

$$P_{H,L} = (-0.00365N_{H,L} - 0.00124N_{H,L}^{-1} + 0.00601)^{-1} \quad (24)$$

2. Heat pump unit heating

By the same token, the relationship between the heating $COP_{H,R}$ and the load rate ($N_{H,R}$) of the heat pump unit is as follows:

$$COP_{H,R} = -20.2303N_{H,R}^2 + 34.5748N_{H,R} - 10.9049 \quad (25)$$

Combined with the rated heat of the unit, the analysis and calculation show the change in power consumption ($P_{H,R}$) with the load rate ($N_{H,R}$) under the heating condition of the heat pump unit:

$$P_{H,R} = (-0.00575N_{H,R} - 0.0031N_{H,R}^{-1} + 0.00982)^{-1} \quad (26)$$

3.4. Mathematical Model of Gas Boiler Subsystem

This project chooses two units with a rated heat output of 12.6 MW, a gas consumption of 1186 Nm³/h, and a burner electric power of 46 kW for the sixth generation Y HZRQ-L1080 ultra-low nitrogen condensing vacuum hot water system. Detailed design performance parameters can be found in Table 14.

Table 14. Performance parameters of gas boiler.

Performance Parameter	Rated Heating Quantity MW	Gas Consumption Nm ³ /h	Distribution Power kW	Heat Efficiency %	Source V/Hz	Modulation of Combustion
YHZRQ-L1080	12.6	1186	46	97	380/50	Frequency conversion electronic ratio adjustment

According to the selection manual and the data provided by the merchants, the scatter plot is drawn and the data are fitted, as shown in Figure 12. The relationship between the load ratio (N_B) and thermal efficiency (η_B) of the gas boiler unit is obtained:

$$\eta_{B1} = \eta_{B2} = -15.142N_B^6 + 62.419N_B^5 - 104.811N_B^4 + 91.488N_B^3 - 43.735N_B^2 + 10.816N_B - 0.0972 \quad (27)$$

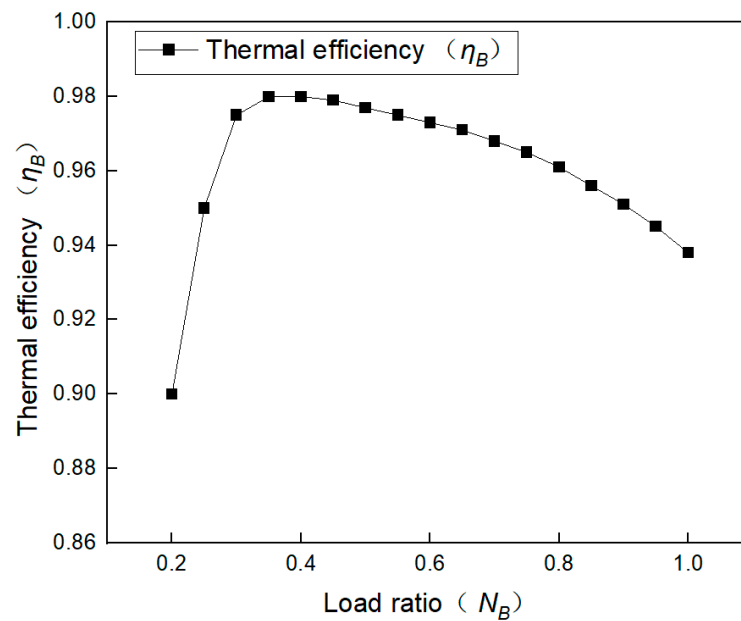


Figure 12. Relationship between load rate and thermal efficiency of gas-fired boiler units.

Combining the gas consumption equation as gas consumption = boiler output/(fuel calorific value \times boiler thermal efficiency), the gas consumption under varying boiler conditions is calculated and analyzed. The relationship between boiler fuel consumption and unit load rate is derived as:

$$G_{B1} = G_{B2} = (-0.01202N_B^5 + 0.0495N_B^4 - 0.08318N_B^3 + 0.07261N_B^2 - 0.0347N_B + 0.00858 - 0.000077N_B^{-1})^{-1} \quad (28)$$

Due to the low power consumption of the boiler, its impact on the system is negligible, so it is assumed that the power of the gas boiler remains unchanged in the dynamic operation process of the variable condition, that is, $P_B = 46$ kW is maintained.

4. Strategy Optimization and Energy Consumption Simulation Analysis of Gas Tri-Supply Composite System

4.1. Traditional Energy Station Cold and Heat Source Energy Consumption Calculation

Chongqing's electricity pricing system follows a time-of-use tariff policy, comprising 8 h for peak, off-peak, and valley periods, respectively, as outlined below:

1. Peak period: 11:00–17:00, 20:00–22:00. Among them, in July and August in summer and in December and January in winter, 12:00–14:00 is the sharp period.
2. Flat period: 08:00–11:00, 17:00–20:00, and 22:00–24:00.
3. Valley period: 00:00–08:00.

The price of the sharp period is 1.2246 yuan/kWh; the peak price is 1.0205 yuan/kWh; the flat price is 0.6378 yuan/kWh; the valley price is 0.2424 yuan/kWh.

The conventional system consists of a chiller unit and a boiler. During summer, a centrifugal chiller is used for cooling, while a gas boiler is employed for heating in winter, following the principle of operating the units at high loads.

Combined with the annual load rate statistics (Tables 2 and 4) and electricity price structure, the annual energy consumption and cost of the traditional system are calculated in Table 15.

The traditional system utilizes high-efficiency centrifugal chiller refrigeration during summer and high-efficiency gas-fired boiler heating during winter. The total annual power consumption amounts to 10.619 million kWh, with an associated energy cost of 8.387 million yuan. Gas consumption stands at 3.482 million Nm^3 , with an energy cost of 7.221 million yuan. During the cooling season, energy is primarily utilized in the form of electricity, with power consumption totaling 10.465 million kWh and an associated energy consumption

cost of 8.272 million yuan. Electricity consumption and energy costs during the cooling season account for 98.5% and 52.9% of the total annual electricity consumption and energy costs, respectively. During the heating season, gas serves as the primary energy source, with lower electricity consumption. Gas consumption during the heating season amounts to 3.482 million Nm³, with a corresponding power consumption of 154,000 kWh and energy cost of 7.337 million yuan. Gas consumption, electricity consumption, and energy costs during the heating season represent 100.0%, 1.5%, and 47.1% of the total annual operating gas consumption, electricity consumption, and energy costs, respectively.

Table 15. Annual energy consumption and cost of traditional cold and heat source system.

Electricity Price Period	Time	Cooling Season			Heating Season		
		Gas Consumption (Nm ³)	Power Consumption (kWh)	Energy Consumption Cost (Yuan)	Gas Consumption (Nm ³)	Power Consumption (kWh)	Energy Consumption Cost (Yuan)
Valley	0:00	0	151,174.19	36,644.62	55,887.92	3330.00	116,718.73
	1:00	0	142,912.56	34,642.00	56,805.99	3330.00	118,622.83
	2:00	0	141,107.94	34,204.56	57,741.28	3330.00	120,562.60
	3:00	0	141,108.81	34,204.78	58,794.50	3330.00	122,746.99
	4:00	0	143,521.30	34,789.56	59,977.58	3330.00	125,200.69
	5:00	0	147,003.45	35,633.64	61,167.86	3330.00	127,669.33
	6:00	0	149,839.80	36,321.17	62,258.03	3330.00	129,930.34
Flat	7:00	0	150,003.02	36,360.73	62,749.99	3330.00	130,950.68
	8:00	0	146,987.44	93,748.59	65,421.42	3330.00	137,807.89
	9:00	0	404,889.79	258,238.71	278,527.95	10,141.00	584,134.91
Peak	10:00	0	438,182.43	279,472.75	237,639.98	10,078.00	499,293.08
	11:00	0	558,551.86	570,002.17	229,269.18	9430.00	485,127.59
	12:00	0	705,045.55	719,498.98	228,266.80	9430.00	483,048.66
	13:00	0	727,839.98	742,760.70	206,351.29	8986.00	437,142.80
	14:00	0	768,673.43	784,431.23	228,374.27	7376.00	481,175.45
	15:00	0	848,550.01	865,945.29	180,595.06	7691.00	382,402.83
Flat	16:00	0	909,939.24	928,592.99	196,329.70	8986.00	416,358.02
	17:00	0	953,805.17	608,336.94	197,262.28	8986.00	414,853.25
	18:00	0	937,874.29	598,176.22	191,071.80	8986.00	402,014.18
Peak	19:00	0	752,123.10	479,704.11	193,008.51	8986.00	406,030.92
	20:00	0	506,826.23	517,216.17	208,058.34	8986.00	440,683.22
Flat	21:00	0	355,041.30	362,319.65	247,923.59	9430.00	523,816.84
	22:00	0	148,574.68	94,760.93	57,664.48	3330.00	121,720.01
Total	23:00	0	135,858.85	86,650.77	61,310.62	3330.00	129,282.09
			0	10,465,434.42	8,272,657.28	3,482,458.44	154,122.00
Summary throughout the year		Total gas consumption	3,482,458.44	Total power consumption	10,619,556.42	All-in cost	15,609,951.20

In this project, the traditional cooling and heating system adopts a configuration of chiller units and gas boilers, powered by electricity and natural gas. From Figure 13, it can be seen that electricity is the main energy source consumed in summer, while gas is the primary energy source consumed in winter. From Figure 13a, it can be observed that the variation in traditional cooling and heating source systems is consistent with the load variation, with the highest consumption occurring during peak electricity price periods. During summer, the cooling load significantly exceeds the heating load in winter, leading to high electricity consumption and costs for the chiller units. Conversely, during winter, although the heating load is lower than the cooling load, the efficiency of gas boilers is lower compared to chiller units, resulting in high gas consumption. As a result, numerical simulation results indicate that the operating costs between the cooling and heating seasons

do not differ significantly. Therefore, it can be observed that traditional cooling and heating systems have significant potential for improvement during the heating season.

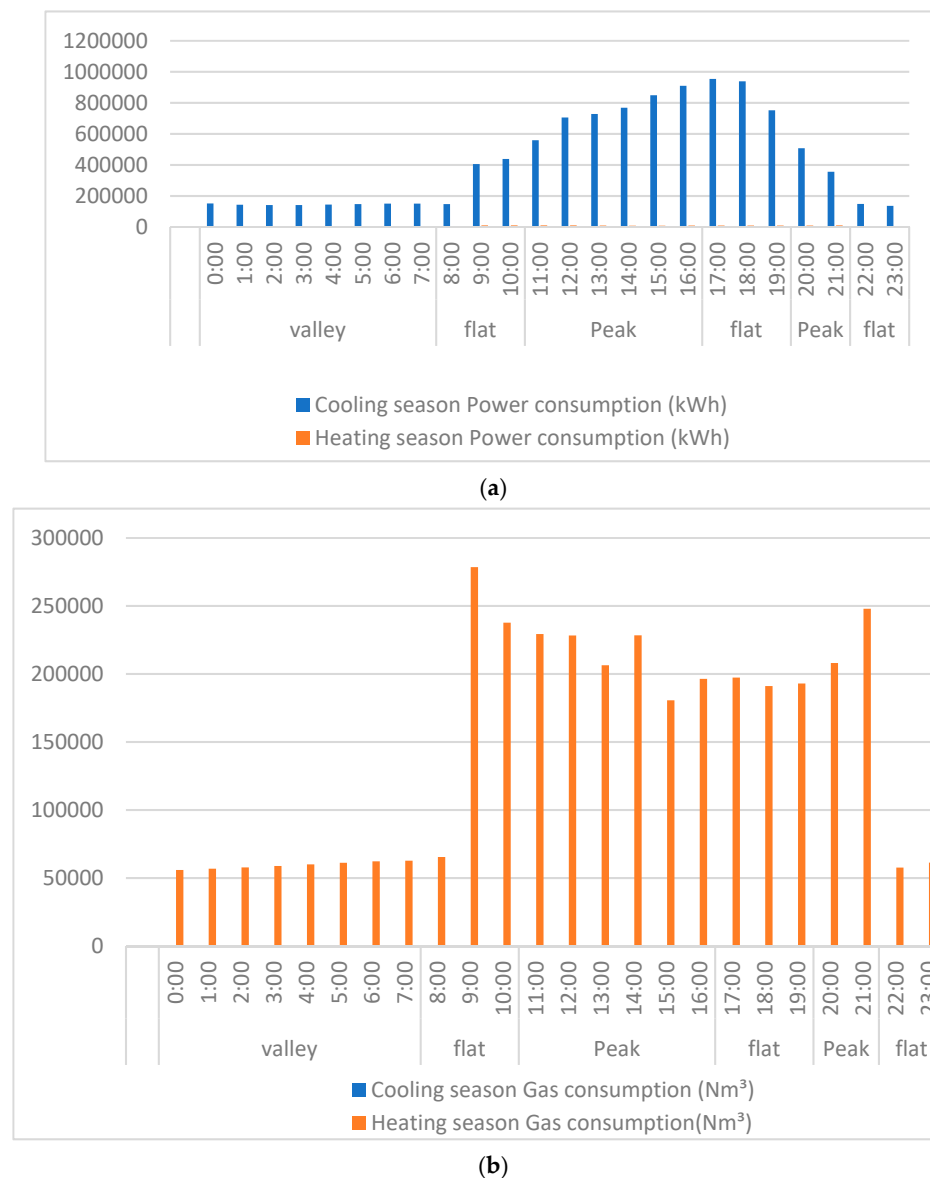


Figure 13. Energy consumption in the hot and cold seasons for conventional hot and cold source systems of (a) electricity consumption and (b) gas consumption.

4.2. Operation Strategy of Gas Tri-Supply Composite Energy System

The composite system of the project comprises the gas tri-supply, ice storage, heat pump, and boiler subsystems. The operation and adjustment of the load system are complex, with various combination methods necessary to address load fluctuations throughout the day. During summer, the ice storage system is preferred due to its ability to regulate peak loads. Furthermore, the price difference between peak and off-peak hours is considered to enhance the project's economy. Based on the capacity of the aforementioned equipment, when the load rate reaches approximately 23%, both the triple-donor subsystem and the heat pump subsystem operate at maximum capacity. The triple-donor subsystem can generate electricity and reduce electricity costs during both cooling and heating processes. However, its efficiency is inferior to that of the heat pump subsystem, which is influenced by factors such as the grid connection mode, electricity tariffs, and gas prices. Thus, the prioritization between the triple-donor subsystem and the heat pump subsystem

depends on both the load rate and electricity prices. During winter, priority is given to heat storage. Similarly, the prioritization is linked to the load rate, electricity prices, and gas prices. The system's control strategy is optimized for optimal economic performance.

4.2.1. Analysis of Summer Control Strategies

In the refrigeration schematic diagram of the gas tri-supply system, as depicted in Figure 14, the heat pump unit (R (L)-1-5), lithium bromide absorption unit (X-1-2), centrifugal unit (L-1), and dual-operating centrifugal unit (S-1-5) are capable of operating to produce chilled water. The dual-condition unit releases cooling capacity through the refrigeration plate for BH-1 and the ice storage tank for BH-2. Additionally, the heat pump unit, lithium bromide absorption unit, centrifugal unit, and refrigeration board for BH-1 operate in parallel before running in series with the ice melting plate for BH-2.

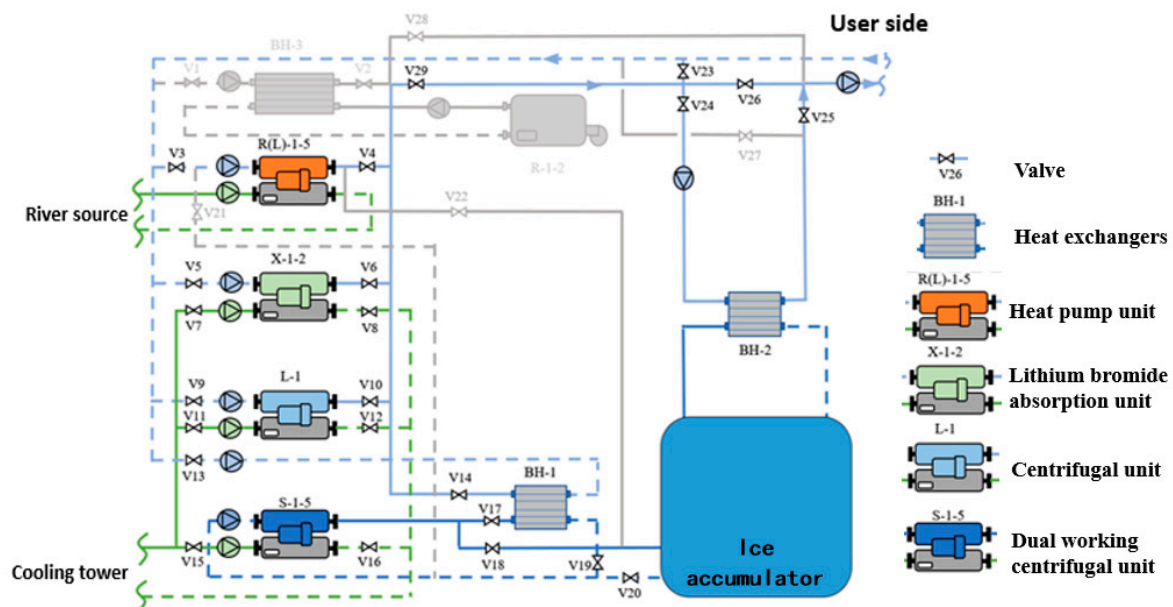


Figure 14. Schematic diagram of composite cold and heat source system.

1. The ice storage subsystem is preferred

During the night power valley price stage, unit S-1-5 operates with valves V15, V16, V18, and V20 open, and the corresponding ice-making pumps and cooling pumps store ice. During the day, the night cold storage capacity is rationally allocated during the peak period of power supply. If there is any surplus after the distribution, then V23, V24 and V25 are opened preferentially to release the ice storage tank for further cooling.

2. Analysis of triple-donor subsystem and heat pump subsystem

In the ice storage subsystem, as the cooling load increases, the triple-supply subsystem or heat pump subsystem is utilized for cooling, followed by the centrifugal unit and dual-operating unit. The priority cost of the triple-supply subsystem and heat pump subsystem varies with different load rates and electricity prices. Consequently, the priority scheme between the triple-supply subsystem and the heat pump subsystem at each load rate is compared. Once the cooling load rate of the system reaches 23.36%, both the heat pump subsystem and the triple-supply subsystem operate at full capacity. Therefore, the operational priority of the subsystem prior to reaching the 23.36% cooling load rate is analyzed, and a relationship diagram between the operational cost and the cooling load rate for each price period is obtained.

It is evident from Figure 15 that during the valley price stage of electricity, utilizing the heat pump subsystem initially yields superior economic benefits across all load rates. During the electricity price parity stage, the operational cost priority of the heat pump

subsystem is lower when the load rate is below 13.72%, whereas the operational cost priority of the triple supply is lower when the load rate exceeds 13.72%. Similarly, during the electricity price peak stage, the operational cost priority of the heat pump subsystem is lower when the load rate is below 7.97%, and conversely, the priority shifts to the triple-supply subsystem when the load rate exceeds 7.97%. If the load rate falls below 7.11%, then the operational cost priority favors the heat pump subsystem, whereas if the load rate surpasses 7.11%, then the priority shifts to the triple-supply subsystem.

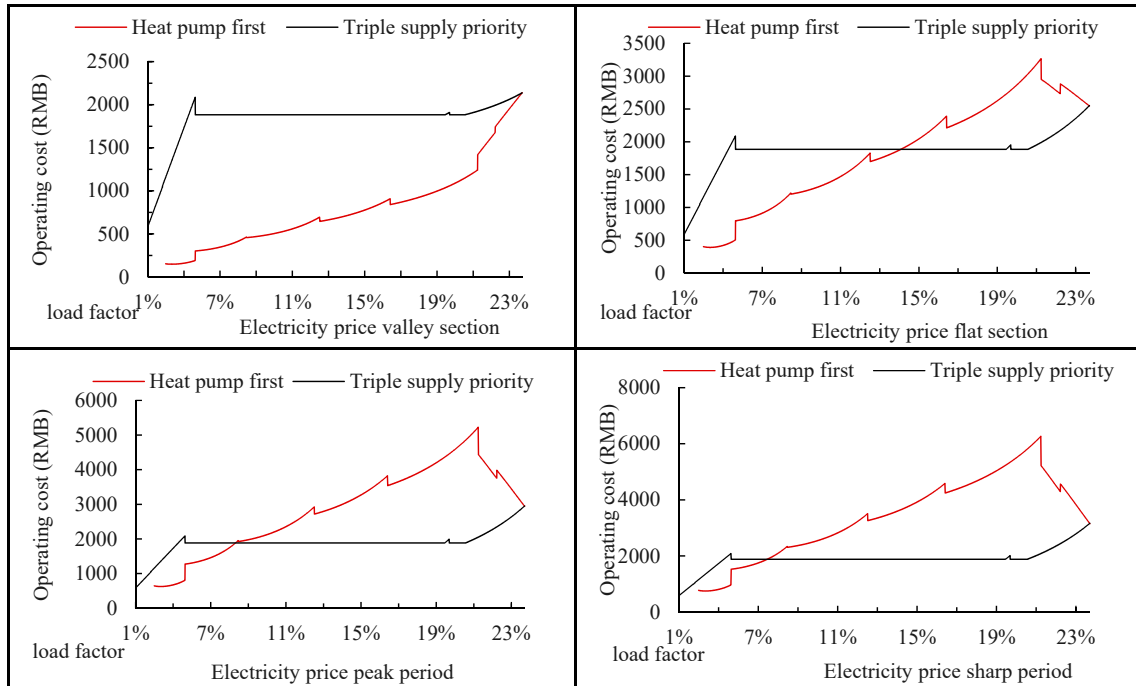


Figure 15. Relationship diagram between operation cost and cooling load rate in each electricity price period.

The priority sequence of the gas tri-supply subsystem and the heat pump subsystem significantly impacts operational costs mainly due to peak/off-peak electricity pricing policies and subsystem energy efficiency. The gas tri-supply subsystem, utilizing natural gas with relatively stable prices, exhibits lower efficiency compared to the heat pump subsystem. Conversely, the heat pump subsystem, relying on electricity, boasts higher efficiency but is subject to peak/off-peak electricity pricing policies. The coupled influence of these two factors affects operational costs, thus necessitating decoupling research on the aforementioned factors to establish a reasonable priority sequence.

Therefore, according to the simulation results and the principle of high load operation of the unit, the optimal operation strategy of summer refrigeration is proposed from the perspective of optimal economy, as in Table 16.

Table 16. Summer control strategies of composite cold and heat source system.

Load Factor	<2.00%	2.00~7.10%	7.11~7.97%	7.98~13.72%	13.73~22.36%
Valley Section	Ice storage first, heat pump second				
Flat Area	Ice storage is first, triple supply is second	Ice storage first, heat pump second			Ice storage is first, triple supply is second
Peak Section		Ice storage first, heat pump second		Ice storage is first, triple supply is second	
Sharp Section	Ice storage first, heat pump second		Ice storage is first, triple supply is second		

4.2.2. Analysis of Winter Control Strategies

The schematic diagram of the composite system is depicted in Figure 16. During heating conditions, the gas boiler (R-1-2), heat pump unit (R (L)-1-5), and lithium bromide absorption unit (X-1-2) are capable of producing air-conditioning hot water. Specifically, the boiler generates air-conditioning hot water via the heating plate for BH-3, while the heat pump unit can store water heat during the night and produce hot water through the plate for BH-2. Initially, the hot water plate for BH-3, the heat pump unit, and the lithium bromide absorption unit operate in parallel and subsequently operate in series with the plate for BH-2.

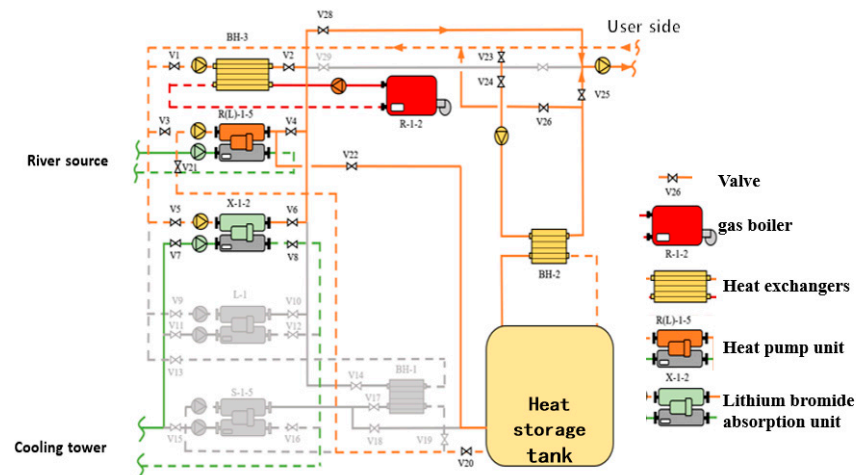


Figure 16. Schematic diagram of the heating operation of the composite cold and heat source system.

1. Water heat storage subsystem is preferred

During the off-peak electricity pricing period at night, unit S-1-5 is activated, heat pump unit R (L)-1-3 is operational, and valves V20, V21, and V22 are opened for tank heat storage. During the daytime, water heat stored in the tank is redistributed to the peak period, sink heat release is prioritized, and valves V23, V24, and V25 are kept closed, allowing only tank heat release.

2. Analysis of the opening sequence of the triple-donor subsystem and the heat pump subsystem

The water heat storage subsystem serves as the primary heating system. As the heat load increases, the gas tri-supply subsystem or heat pump subsystem is utilized for heating, with the gas boiler serving as a final option. Depending on the load rate and electricity price, the priority cost of the gas tri-supply subsystem and heat pump subsystem varies. Thus, a comparison is made between the priority schemes of the gas tri-supply subsystem and the heat pump subsystem at various load rates. At a heat load rate of 45.84% in the system, both the heat pump subsystem and the gas tri-supply subsystem operate at full capacity. Therefore, an analysis of the operation priority of the subsystem before reaching this heat load rate is conducted, and the relationship between operation cost and heat load rate for each pricing period is depicted in Figure 16.

According to Figure 17, during the electricity valley price stage, utilizing the heat pump subsystem can consistently yield superior economic benefits across all load rate scenarios. During the electricity price parity phase, if the load rate is below 29.02%, then the operational cost priority favors the heat pump; however, if the load rate exceeds 29.02%, the operational cost priority shifts to the gas tri-supply subsystem. Likewise, during the peak stage of electricity prices, if the load rate falls below 19.08%, the operational cost priority favors the heat pump; however, if the load rate exceeds 19.08%, then the operational cost priority shifts to the gas tri-supply subsystem. In the electricity sharp price stage, if the load rate is below 14.78%, then the operational cost priority favors the heat pump;

however, if the load rate exceeds 14.78%, then the operational cost priority shifts to the triple-supply subsystem.

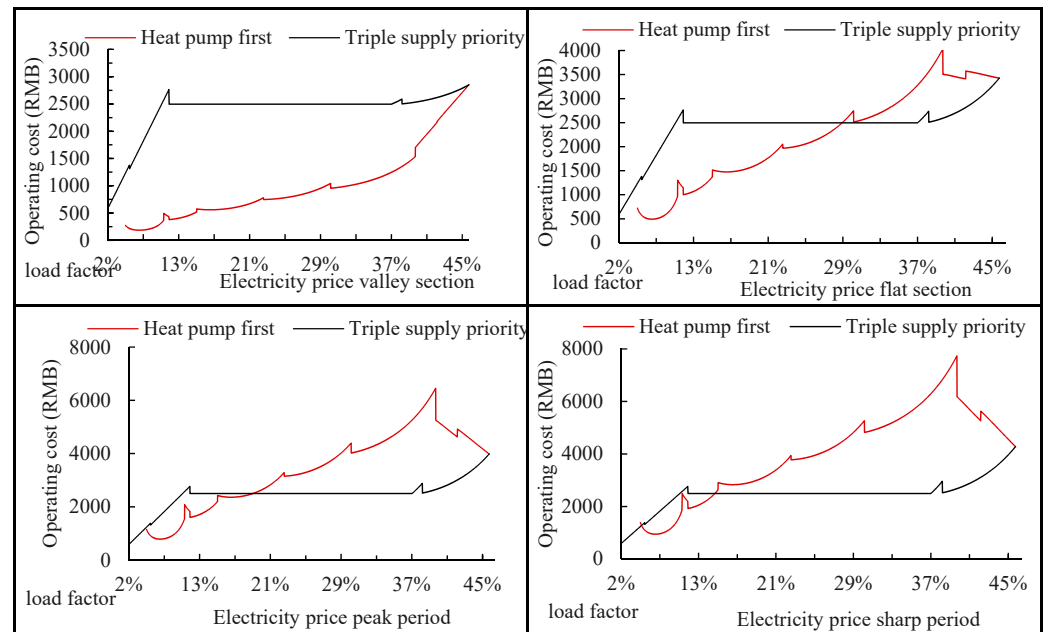


Figure 17. Relationship diagram between operating cost and heat load rate in each electricity price period.

Therefore, according to the simulation results and the high load operation principle of the unit, the best operation strategy of winter heating is proposed from the perspective of economy, as in Table 17.

Table 17. Winter control strategy table of composite cold and heat source system.

Load Factor	<4.00%	4.00~17.48%	17.49~19.80%	19.81~29.02%	29.03~45.84%
Valley Section	Water heat storage first, heat pump second				
Flat Section	Water heat storage is preferred, triple supply is second	Water heat storage first, heat pump second			Water heat storage is preferred, triple supply is second
Peak Section		Water heat storage first, heat pump second		Water heat storage is preferred, triple supply is second	
Sharp Section	Water heat storage first, heat pump second		Water heat storage is preferred, triple supply is second		

4.3. Annual Energy Consumption Analysis of Gas Tri-Supply Composite System

4.3.1. Gas Tri-Supply Composite System Energy Consumption Calculation

According to the aforementioned control strategy, combined with the annual load rate statistics (Tables 2 and 4) and electricity price structure, the annual energy consumption and cost of the composite system operation are calculated. Table 18 shows the results.

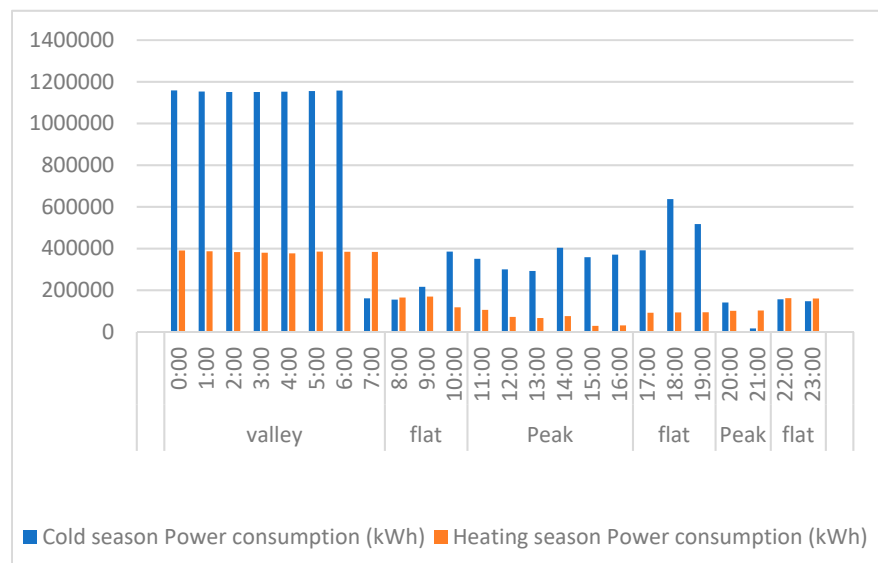
By employing the composite energy system, the optimal strategy can be proposed through rigorous optimization research. Under the optimal strategy, the yearly expenses are calculated. Both the gas triple-supply subsystem and the gas boiler subsystem operate on gas, resulting in an annual gas consumption of 2.198 million Nm³, with the associated costs amounting to 4.426 million yuan. Annually, the power consumption totals 17.78 million kWh, incurring an electricity cost of 8.813 million yuan. The total annual operating cost

amounts to 13.239 million yuan. Specifically, during the cooling season, gas consumption, power consumption, and overall energy consumption represent 42.98%, 73.54%, and 60.29% of the total energy consumption, respectively, while during the heating season, gas consumption, power consumption, and overall energy consumption constitute 57.02%, 26.46%, and 39.71%, respectively.

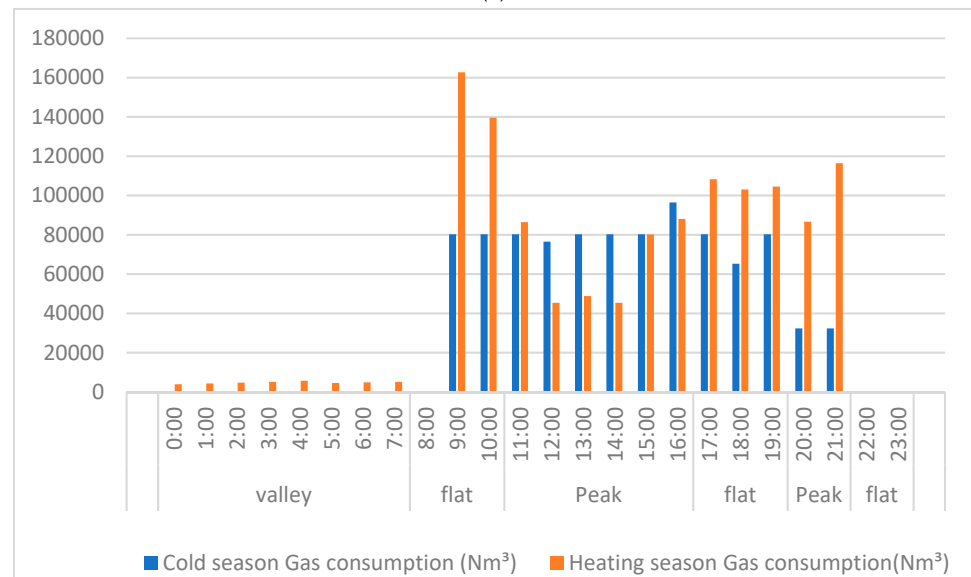
Table 18. Annual energy consumption and cost of gas tri-supply composite system.

Electricity Price Period	Time	Cold Season			Heating Season		
		Gas Consumption (Nm ³)	Power Consumption (kWh)	Energy Consumption Cost (Yuan)	Gas Consumption (Nm ³)	Power Consumption (kWh)	Energy Consumption Cost (Yuan)
Valley	0:00	0.00	1,158,820.60	280,898.11	3893.76	390,207.67	104,616.66
	1:00	0.00	1,153,163.50	279,526.83	4289.76	386,483.00	104,733.90
	2:00	0.00	1,150,730.05	278,936.96	4691.04	383,166.48	104,963.67
	3:00	0.00	1,150,730.66	278,937.11	5145.12	379,924.28	105,347.47
	4:00	0.00	1,152,493.10	279,364.33	5652.00	376,872.38	105,913.42
	5:00	0.00	1,155,240.96	280,030.41	4564.32	385,193.84	105,128.67
	6:00	0.00	1,157,649.69	280,614.28	4902.24	384,253.84	105,771.30
Flat	7:00	0.00	161,186.40	39,071.58	5108.16	383,545.09	106,129.95
	8:00	0.00	155,083.23	98,912.09	0.00	164,573.26	104,964.83
	9:00	80,269.68	215,941.13	304,206.57	162,713.93	169,752.75	527,419.39
Peak	10:00	80,269.68	384,919.00	411,980.66	139,547.99	118,198.85	434,862.86
	11:00	80,269.68	350,385.62	524,047.84	86,397.43	105,925.80	330,657.05
	12:00	76,471.60	299,848.22	507,213.55	45,370.04	71,660.58	199,236.16
	13:00	80,269.68	292,537.81	507,061.68	48,748.66	66,340.06	201,788.49
	14:00	80,269.68	403,376.13	578,124.66	45,370.04	75,471.03	193,891.41
	15:00	80,269.68	358,361.81	532,187.54	80,121.56	28,717.19	235,699.04
Flat	16:00	96,415.88	370,654.93	578,219.90	88,077.80	30,935.05	258,457.62
	17:00	80,269.68	391,445.41	416,143.20	108,232.63	91,462.04	337,141.74
	18:00	65,260.40	636,811.98	541,508.75	103,071.61	93,311.93	325,026.82
Peak	19:00	80,269.68	517,249.35	496,380.95	104,546.94	93,824.01	329,153.88
	20:00	32,292.40	141,233.26	211,102.98	86,682.45	101,352.29	326,724.00
Flat	21:00	32,292.40	16,512.10	83,825.03	116,437.26	102,872.79	404,924.06
	22:00	0.00	156,412.24	99,759.73	0.00	161,680.26	103,119.67
Total	23:00	0.00	147,179.92	93,871.35	0.00	160,099.65	102,111.56
		944,890.12	13,077,967.10	7,981,926.09	1,253,564.74	4,705,824.12	5,257,783.65
Summary throughout the year		Total gas consumption	2,198,454.86	Total power consumption	17,783,791.22	All-in cost	13,239,709.74

As can be seen from Figure 18 and Table 18, the gas tri-supply composite system uses gas consumption from the gas tri-supply subsystem in both winter and summer. The gas consumption of the triple-supply subsystem in winter is greater than that in summer, indicating that the heating output of the triple-supply subsystem in winter is greater than the cooling output in summer, which is due to the fact that the cooling load in summer is mainly borne by the chiller, the ice storage subsystem, and the heat pump subsystem. As can be seen from Figure 18a, electricity consumption in summer and winter is mainly concentrated in the valley phase, which indicates the obvious role of the ice storage subsystem in shifting peaks and filling valleys. Compared with the traditional cold and heat source system, even though the power consumption is greater, the operation cost is lower.



(a)



(b)

Figure 18. Energy consumption in the hot and cold seasons for gas tri-supply composite systems of (a) electricity consumption and (b) gas consumption.

4.3.2. Comparative Evaluation of Energy Consumption of Gas Tri-Supply System

Under the optimal operational strategy, an analysis and comparison are conducted between the composite system and the traditional cold and heat source systems. Gas and electricity are converted into standard coal using the standard coal conversion method. The detailed findings are presented in Table 19.

In comparison to the traditional cooling and heat source systems, the combined gas tri-supply system consumes an additional 7.164 million kWh, resulting in an operating cost increase of 426,000 yuan. The annual gas consumption of the combined gas tri-supply system decreases by 1.284 million Nm^3 , leading to a reduction in operating costs by 2.911 million yuan. Looking at it from a comprehensive point of view, utilizing the combined gas tri-supply system can result in annual operating cost savings of 2.37 million yuan, albeit with an increase of 574,000 kg in annual standard coal consumption. The combined gas tri-supply system utilizes the heat pump subsystem and gas tri-supply subsystem for heating compared to a conventional system, and therefore consumes less

natural gas but more electricity throughout the year. Through energy storage technology and peak/off-peak electricity pricing policies, it can reduce the cost of electricity for the combined gas tri-supply system. Therefore, the combined annual operating cost of the combined gas tri-supply system is lower.

Table 19. Comparison table of the energy consumption and cost of the cold and heat source system.

	Annual Power Consumption (Ten Thousand kWh)	Annual Electricity Cost (Ten Thousand Yuan)	Annual Gas Consumption (Ten Million Nm ³)	Annual Gas Cost (Ten Thousand Yuan)	Annual Total Operating Expenses (Ten Thousand Yuan)	Standard Coal Quantity (Ten Thousand Kg)
Traditional system	1061.9	827.2	348.2	733.7	1560.9	892.9
Gas tri-supply composite system	1778.3	881.3	219.8	442.6	1323.9	950.3

4.4. Performance Analysis of Gas Tri-Supply Composite System

4.4.1. Peak-Shifting and Valley-Filling Ability of Gas Tri-Supply System

According to the distribution of power consumption in the annual cooling and heating season, the peak-shifting capacity during operation is calculated and analyzed. In order to more directly reflect the peak-shifting capacity of the system, natural gas consumption is converted into power consumption according to the relationship between gas price and electricity price, and the annual power consumption in the cooling and heating season is further calculated and analyzed. The results are shown in Table 20.

Table 20. Peak-shifting and valley-filling capacity table.

Index of Correlation	Peak Filling Capacity in Cooling Season	Peak Shifting Capacity during Heating Season
Total power consumption (kWh)	15,469,429.75	9,116,254.95
Peak segment power consumption (kWh)	3,368,073.8	2,090,771.78
Valley consumption (kWh)	8,240,014.95	3,476,093.46
Peak-shifting power rate (%)	49.68	46.26
Valley electricity utilization rate (%)	53.27	38.13

The peak-shifting rate in the cooling season is 49.68%, and the valley power utilization rate is 53.27%. It can be seen that the peak-shifting capacity of the gas tri-supply composite system is obvious. In the heating season, the peak-shifting rate is 46.26%, and the valley power utilization rate is 38.13%, which also has good peak-shifting and valley-filling capacities. In this project, the energy storage system adopts both ice storage and water storage systems, storing energy during off-peak hours and releasing it during peak hours. The peak-shaving and valley-filling capabilities of the energy storage system depend on the design of the storage capacity and control strategy. This project adopts a strategy prioritizing energy storage to maximize the peak-shaving and valley-filling capabilities of the energy storage system.

4.4.2. Power Generation Analysis of Gas Tri-Supply Subsystem

In the current gas tri-supply system, power plants, and self-owned power generation systems in China, the primary operational modes are grid-connected and independent. Independent operation, also known as “isolated grid operation”, involves establishing a separate grid to independently fulfill the electricity requirements of the enterprise. Grid-connected operation is the prevailing mode in the current tri-generation system, which encompasses two power exchange methods: “grid-connected without grid access” and “grid-connected with grid access”. “Grid-connected without grid access” denotes the tri-generation system generating electricity for internal consumption. If the generated electricity fails to meet the system’s demand, then supplementary electricity is sourced from the public grid to ensure system stability. However, surplus electricity generated

beyond the system's requirements cannot be exported. Grid access operation frequently results in unstable fluctuations in the public grid due to grid policies, posing potential safety hazards. Consequently, the majority of tri-generation systems presently operate in a grid-connected configuration without grid access. In order to ensure the stability and safety of the grid, this project also adopts the grid-connected mode of operation without grid access. Under this operation mode, the annual power generation of the hybrid system (Q_P), electricity downloaded from the public grid (Q_D), electricity uploaded to the public grid (Q_U), and revenue from uploading electricity (I_U) are as follows:

$$\begin{cases} Q_P = \sum_{t=1}^{8760} Q_{P,T} \\ Q_D = \sum_{t=1}^{8760} Q_{D,T} \\ Q_U = 0 \\ I_U = 0 \end{cases} \quad (29)$$

Combined with the mathematical model in Section 2, the annual power production of the triple-supply subsystem of this project is calculated and analyzed, and the calculation results are shown in Table 21 under the optimal control strategy:

Table 21. Calculation of the annual power production of the triple-supply subsystem.

	Grid-Connected and Off-Grid	Optimized Control Strategy
Gas consumption (Nm ³)	G _{gas}	2,198,454.86
Annual power generation (kW)	Q _P	7,360,298.01
Downloaded power (kW)	Q _D	17,783,791.22
Upload battery level (kW)	Q _U	0.00
Upload earnings (yuan)	I _U	0.00

Based on the calculation results above, the triple-supply system, when operated optimally, generates 7.360 million kWh of electricity annually, representing 29.3% of the total annual electricity consumption. Concurrently alleviating strain on the power grid, it lowers annual operating energy costs and yields favorable economic returns. Calculated based on the average electricity price in Chongqing, the power output value of this project's cogeneration system amounts to 4.662 million yuan.

The electricity generation of the gas tri-supply subsystem is related to the operating load and control strategy. Section 4.2 discusses the control strategy of the gas tri-supply subsystem with the aim of minimizing operating costs. Under this control strategy, the tri-generation subsystem's annual electricity generation can bring good returns, further enhancing the project's economic viability from a holistic perspective. Additionally, the electricity generation of the gas tri-supply subsystem has great potential for alleviating peak loads on the power grid, improving the energy station's ability for flexible power consumption.

5. Conclusions

This article examines a tri-generation composite regional energy supply system in Chongqing, China, analyzing its control strategy optimization, annual energy consumption, and economic performance. By conducting load simulations and mathematical modeling, an economically optimal control strategy for the tri-generation composite system is proposed, and the annual energy consumption and operating costs of the project under this optimization strategy are calculated. Through comparison with the annual energy consumption of the traditional cold and heat source system in the energy station, the economic superiority and other outstanding performance metrics of the tri-generation composite system are identified. The main conclusions of this article are as follows:

1. The start-stop sequence, load ratio, and electricity price of the gas tri-supply subsystem and heat pump subsystem utilized in this project exhibit complex interdepen-

- dencies. This article examines the operational priority between the gas tri-supply subsystem and heat pump subsystem under a priority strategy of cold and heat storage and proposes an optimal operational strategy.
2. Under the optimal control strategy, the gas tri-supply composite system employed in this project demonstrates superior economic benefits compared to the traditional cold and heat source systems in the regional energy station, resulting in an annual savings of 2.37 million yuan. In terms of standard coal equivalents, the gas tri-supply composite system consumes an additional 574,000 kg of standard coal when accounting for the conversion of electricity and gas.
 3. The regional gas tri-supply composite system implemented in this project effectively utilizes the ice storage and heat storage systems to achieve peak shaving during both the cooling and heating seasons. During the cooling season, the peak-shaving rate reaches 49.68%, with a valley utilization rate of 53.27%. Similarly, during the heating season, the peak-shaving rate stands at 46.26%, accompanied by a valley utilization rate of 38.13%. In addition to its favorable economic performance, this system effectively mitigates the challenge of high peak power loads.
 4. The gas tri-supply subsystem implemented in this project utilizes a grid-connected mode without direct grid access for power generation. Through optimized strategies, it generates a total of 7.360 million kWh of electricity annually, representing 29.3% of the year-round total electricity consumption. This approach alleviates strain on the power grid and yields greater economic benefits for the regional energy station.

Through the analysis of regional gas tri-supply composite systems, it is evident that they exhibit favorable economic viability. This could be informative for the future construction of regional energy stations. Additionally, optimizing control strategies may provide insights for managing the operation of already established regional energy stations. However, this study has its limitations. It relies on numerical simulations and lacks a comprehensive analysis of actual operational data from energy stations. Moreover, the focus of this study predominantly lies on economic aspects, with insufficient analysis of other advantages of regional gas tri-supply composite systems. The following areas could be explored in future research: (1) Focus more on the role of regional gas tri-supply composite systems in accommodating new energy power consumption. (2) As renewable energy technologies advance, more subsystems may integrate, such as photovoltaic power generation, warranting valuable research into these more complex systems. (3) Analyze optimization control strategies using actual operational data from regional energy stations.

Author Contributions: Methodology, J.L. and Y.C.; software, H.S.; formal analysis, Y.C.; investigation, H.Y.; resources, H.Y. and J.Y.; data curation, H.S.; writing—original draft preparation, M.D.; writing—review and editing, M.D. and S.L.; visualization, S.L.; supervision, J.L.; project administration, J.Y. All authors have read and agreed to the published version of the manuscript.

Funding: This research received no external funding.

Data Availability Statement: The original contributions presented in the study are included in the article, further inquiries can be directed to the corresponding author.

Conflicts of Interest: Authors Hao Shen and Jie Yuan were employed by the company Nuclear Industry Jingxiang Construction Group Co., Ltd. The remaining authors declare that the research was conducted in the absence of any commercial or financial relationships that could be construed as a potential conflict of interest.

References

1. Cheng, Y.; Zhang, N.; Wang, Y.; Yang, J.; Kang, C.; Xia, Q. Modeling Carbon Emission Flow in Multiple Energy Systems. *IEEE Trans. Smart Grid* **2018**, *10*, 3562–3574. [[CrossRef](#)]
2. Shenxi, Z.; Danyang, W.; Haozhong, C.; Yi, S.; Kai, Y. Key Technologies and Challenges of Low-carbon Integrated Energy System Planning for Carbon Emission Peak and Carbon Neutrality. *Autom. Electr. Power Syst.* **2022**, *46*, 189–207. [[CrossRef](#)]
3. Wang, Y.Z.; Kang, L.; Zhang, J.; Zhao, W.; Zhu, Y.L. Development history, typical forms and future trends of integrated energy systems. *Acta Energetica Sin.* **2021**, *42*, 84–95. [[CrossRef](#)]

4. Li, X. Current situation and development prospects of China's natural gas market. *Shanghai Gas* **2020**, *6*, 30–33. [[CrossRef](#)]
5. Xian, J.; Lin, Z.; Zhan, N.; Wang, S. Development status and application prospect of distributed natural gas CCHP system in Guangdong. *Chengshi Ranqi* **2018**, *6*, 7–10. [[CrossRef](#)]
6. Liu, Q.; Liao, L.; Ren, H.; Ban, Y.; Yang, J. Investigation on the Development Status of Distributed Energy in Shanghai. *J. Shanghai Univ. Electr. Power* **2015**, *31*, 429–433, 442. [[CrossRef](#)]
7. Li, Z.; Zhao, J.; Shan, D.; Liu, W.; Zhao, Z. Typical Case Analysis of Gas Distributed Energy System. *Distrib. Energy* **2019**, *4*, 32–37. [[CrossRef](#)]
8. Zhang, L.; Jin, Q.; Zhang, W.; Chen, L.; Yang, N.; Chen, B. Risk-involved dominant optimization of multi-energy CCHP-P2G-based microgrids integrated with a variety of storage technologies. *J. Energy Storage* **2024**, *80*, 110260, ISSN 2352-152X. [[CrossRef](#)]
9. Ren, H.; Gao, W.; Ruan, Y. Optimal sizing for residential CHP system. *Appl. Therm. Eng. Des. Process. Equip. Econ.* **2008**, *28*, 514–523. [[CrossRef](#)]
10. Wu, J.-Y.; Wang, J.-L.; Li, S. Multi-objective optimal operation strategy study of micro-CCHP system. *Energy* **2012**, *48*, 472–483. [[CrossRef](#)]
11. Nong, J.; Li, J.; Zhu, S. Hierarchical Coordinated Control Strategy of Microgrid with CCHP System. *South. Power Syst. Technol.* **2016**, *10*, 82–90. [[CrossRef](#)]
12. Tu, Q.; Fan, H.; Wang, H. Bi-level coordination and optimal scheduling method for multi-body distributed integrated energy systems. *Water Resour. Hydropower Eng.* **2023**, *54*, 29–39. [[CrossRef](#)]
13. Chu, S.; Liu, Y.; Xu, Z.; Zhang, H.; Chen, H.; Gao, D. Multi-objective optimization of micro-gas turbine coupled with LCPV/T combined cooling, heating and power (CCHP) system based on following electric load strategy. *Energy Convers. Manag.* **2024**, *299*, 117860, ISSN 0196-8904. [[CrossRef](#)]
14. Hou, Z. Research and Comparison of Regional centralized Cooling and Central Air conditioning Systems. *Enterp. Technol. Dev.* **2011**, *30*, 24–26.
15. Moslehi, K.; Kumar, R. A Reliability Perspective of the Smart Grid. *IEEE Trans. Smart Grid* **2010**, *1*, 57–64. [[CrossRef](#)]
16. Reynders, G.; Lopes, R.A.; Marszal-Pomianowska, A.; Aelenei, D.; Martins, J.; Saelens, D. Energy flexible buildings: An evaluation of definitions and quantification methodologies applied to thermal storage. *Energy Build.* **2018**, *166*, 372–390. [[CrossRef](#)]
17. Baillieul, J.; Caramanis, M.C.; Ilic, M.D. Control Challenges in Microgrids and the Role of Energy-Efficient Buildings [Scanning the Issue]. *Proc. IEEE* **2016**, *104*, 692–696. [[CrossRef](#)]
18. Chen, R.; Li, Z.; Yuan, T. Cold source economic analysis of air conditioning system of an office building complex in Guangzhou. *Zhi Leng* **2023**, *42*, 8–12, 17. [[CrossRef](#)]
19. Xu, P.; Pan, A.; Duan, Z. Analysis of influencing factors on economy of ice storage air conditioning system. *J. Xi'an Univ. Arch. Tech. (Nat. Sci. Ed.)* **2021**, *53*, 109–116. [[CrossRef](#)]
20. Fan, Y.; Long, W. Carbon Dioxide Emissions Reduction Analysis of Ice Storage System. *J. Tongji Univ. (Nat. Sci.)* **2011**, *39*, 105–108, 134. [[CrossRef](#)]
21. Hasnain, S.M.; Alabbadi, N.M. Need for thermal-storage air-conditioning in Saudi Arabia. *Appl. Energy* **2000**, *65*, 153–164. [[CrossRef](#)]
22. Hu, T.; Zhou, Q.; Xiao, R.; Gao, Z.; Zhu, J. An online Optimal Operation Control for Water Storage Ground source Heat pump System. *Acta Sol. Energy Sin.* **2018**, *39*, 496–502.
23. Dai, W.; Xia, W.; Li, B.; Goh, H.; Zhang, Z.; Wen, F.; Ding, C. Increase the integration of renewable energy using flexibility of source-network-load-storage in district cooling system. *J. Clean. Prod.* **2024**, *441*, 140682. [[CrossRef](#)]
24. Cao, J.W.; Huang, S.; Sun, Y. Micro-grid stochastic economic scheduling strategy of ice storage air conditioning group participating in local consumption of landscape. *South. Power Technol.* **2022**, *16*, 68–78.
25. He, H.; Guo, J.; Wang, Y. Research on multi-objective optimization strategy for ice storage air conditioning system for distribution network wind power consumption. *Power Syst. Prot. Control.* **2019**, *47*, 180–187. [[CrossRef](#)]
26. Wang, X.; Kang, X.; Yan, D.; Qin, R. Research on control method of ice storage system in commercial complex based on cold capacity prediction. *Build. Sci.* **2022**, *38*, 7–16+66. [[CrossRef](#)]
27. Wu, L.; Wang, X.; Shang, X.; Yang, Y.; Huo, Q.; Hu, Q. Control Strategy for Ice Storage Air Conditioning under Different Load Operations Throughout the Year. *J. Electr. Power Syst. Autom.* **2019**, *32*, 98–104. [[CrossRef](#)]
28. Shi, Q. Control strategy design and performance analysis of a low carbon and high ratio green energy CCHP (LCHRG-CCHP) system. *Energy Rep.* **2024**, *11*, 4233–4244, ISSN 2352-4847. [[CrossRef](#)]
29. Zhang, W. Research on Operation Performance and Optimization Strategy of Natural Gas CCHP and River Water Source Heat pump Composite System. Bachelor's Thesis, Chongqing University, Chongqing, China, 2019.
30. Li, Y. Operation Strategy Optimization Analysis of Regional Ice Storage Air Conditioning System. Bachelor's Thesis, Chongqing University, Chongqing, China, 2019.
31. Wang, J.; Cao, J.; Zhang, L. Review on application of cold storage and heat storage technology based on distributed energy system. *Energy Storage Sci. Technol.* **2020**, *9*, 1847–1857. [[CrossRef](#)]
32. Qin, Y.; Chen, X.; Wang, H. Application of ice storage air conditioning system in Building Type Distributed energy station. *Gas Heat* **2014**, *34*, 21–24. [[CrossRef](#)]
33. Wang, X.; Jiang, T.; Xu, J.; Deng, Y.; Hu, Y. Research and application of cold storage solution in the natural gas distributed energy station. *Huadian Technol.* **2018**, *40*, 72–76. [[CrossRef](#)]

34. Wang, H.; Zhao, J.; An, Q.; Kang, L. Study on Optimization and Policy Incentives of Distributed Energy System Under Different Building Loads. *Proc. CSEE* **2015**, *35*, 3734–3740. [[CrossRef](#)]
35. Yu, C.; Ye, D.; Zhang, D. Optimization of Operation Mode of Energy System in Gas-fired Combined Cooling, Heating and Power Supply Area in Shanghai. *HVAC* **2021**, *51*, 232–235.
36. Jia, J.; Li, H.; Wu, D.; Guo, J.; Jiang, L.; Fan, Z. Multi-objective optimization study of regional integrated energy systems coupled with renewable energy, energy storage, and inter-station energy sharing. *Renew. Energy* **2024**, *225*, 120328. [[CrossRef](#)]
37. Zuo, Z. Comparison between Gas Engine and Gas Turbine CCHP system. *Gas Heat* **2005**, *25*, 39–42.
38. Wu, J. Optimization Analysis on Operation Strategy of Dynamic Ice Storage System in Energy Station. Bachelor's Thesis, Chongqing University, Chongqing, China, 2021.
39. Shi, L. Research on Optimal Operation of Ice Storage Air Conditioning System Based on online Load Prediction Correction. Bachelor's Thesis, Xi'an University of Architecture and Technology, Xi'an, China, 2002.

Disclaimer/Publisher's Note: The statements, opinions and data contained in all publications are solely those of the individual author(s) and contributor(s) and not of MDPI and/or the editor(s). MDPI and/or the editor(s) disclaim responsibility for any injury to people or property resulting from any ideas, methods, instructions or products referred to in the content.